ACS NANO

www.acsnano.org

ARTICLE

Cecropin A-Derived Peptide for the Treatment of Osteomyelitis by Inhibiting the Growth of Multidrug-Resistant Bacteria and Eliminating Inflammation

Ziao Zhou,[‖] Peng Zhang,[‖] Dinghao Chen, Nan Kong, Huayang Liu, Juan Liang, Kai Huang, and Huaimin Wang*

Cite This: https://doi.org/10.1021/acsnano.4c18858

Read Online

ACCESS | Metrics & More | Article Recommendations | Supporting Information

ABSTRACT: **Osteomyelitis poses substantial therapeutic challenges due to the prevalence of multidrug-resistant bacterial infections and associated inflammation. Current treatment regimens often rely on a combination of corticosteroids and antibiotics, which can lead to complications and impede effective bacterial clearance. In this study, we present CADP-10, a Cecropin A-derived peptide, designed to target methicillin-resistant *Staphylococcus aureus* (MRSA) and multidrug-resistant *Escherichia coli* (MRE), while simultaneously addressing inflammatory responses. CADP-10 self-assembles into nanobacterial net (NBacN) that selectively identify and bind to bacterial endotoxins (LPS and LTA), disrupting membrane integrity and depolarizing membrane potential, which culminates in bacterial death. Importantly, these NBacN are bound to LPS and LTA from dead bacteria, preventing their engagement with TLR receptors and effectively blocking downstream inflammatory pathways. Our assessments of CADP-10 demonstrate good biosafety in both *in vitro* and *in vivo* models. Notably, in a rabbit osteomyelitis model, CADP-10 eliminated MRSA-induced bone infections, mitigated inflammation, and promoted bone tissue regeneration. This research highlights the potential of CADP-10 as a multifunctional antimicrobial agent for the management of infectious inflammatory diseases.**

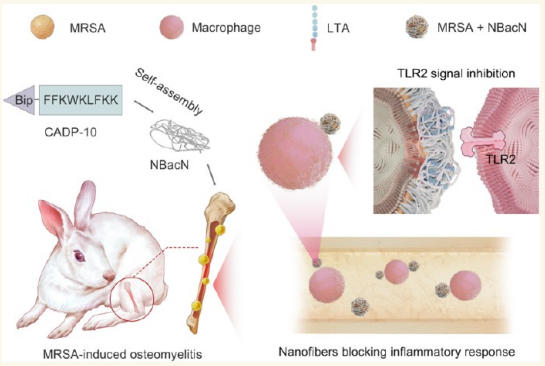

KEYWORDS: *osteomyelitis, endotoxin, TLR receptors, multidrug-resistant bacteria, inflammation*

Osteomyelitis, an infection of bone tissue, arises primarily from bone trauma, the spread of adjacent infected tissue, or bacteriaemia.[1] In the United States, the incidence of osteomyelitis is approximately 22 cases per 100,000 individuals per year, representing a significant healthcare burden.[2] Moreover, this condition can lead to severe complications, including abscess formation, sepsis, organ infections, and, in extreme cases, mortality. Clinically, systemic antibiotic therapy is the standard approach to reduce bacterial load and manage osteomyelitis.[3] However, the misuse and overuse of antibiotics have facilitated the emergence of drug-resistant bacteria, significantly diminishing the effectiveness of conventional treatments.[4,5] The death of bacteria at the infection site often results in the release of endotoxins,[6] which can provoke intense inflammatory responses and cause substantial damage to surrounding tissues, potentially leading to permanent dysfunction.[7] Thus, it is crucial to control both the infection and the associated inflammation as early as possible to mitigate the risks of disability and death. While combining corticosteroids with antibiotics can effectively kill bacteria and suppress inflammation,[8,9] this strategy carries inherent risks, including obstacles to bacterial clearance and the potential for serious complications.[10−12] There is an urgent need for innovative antibacterial agents that can simultaneously target infection and modulate the excessive inflammation triggered by dead bacteria.

In the innate immune system, α-defensin (HD6)[13] and uromodulin (UMOD),[14] expressed and secreted by host cells in the gut or urethra, can recognize and trap invading bacteria

Received: December 27, 2024
Revised: April 4, 2025
Accepted: April 7, 2025

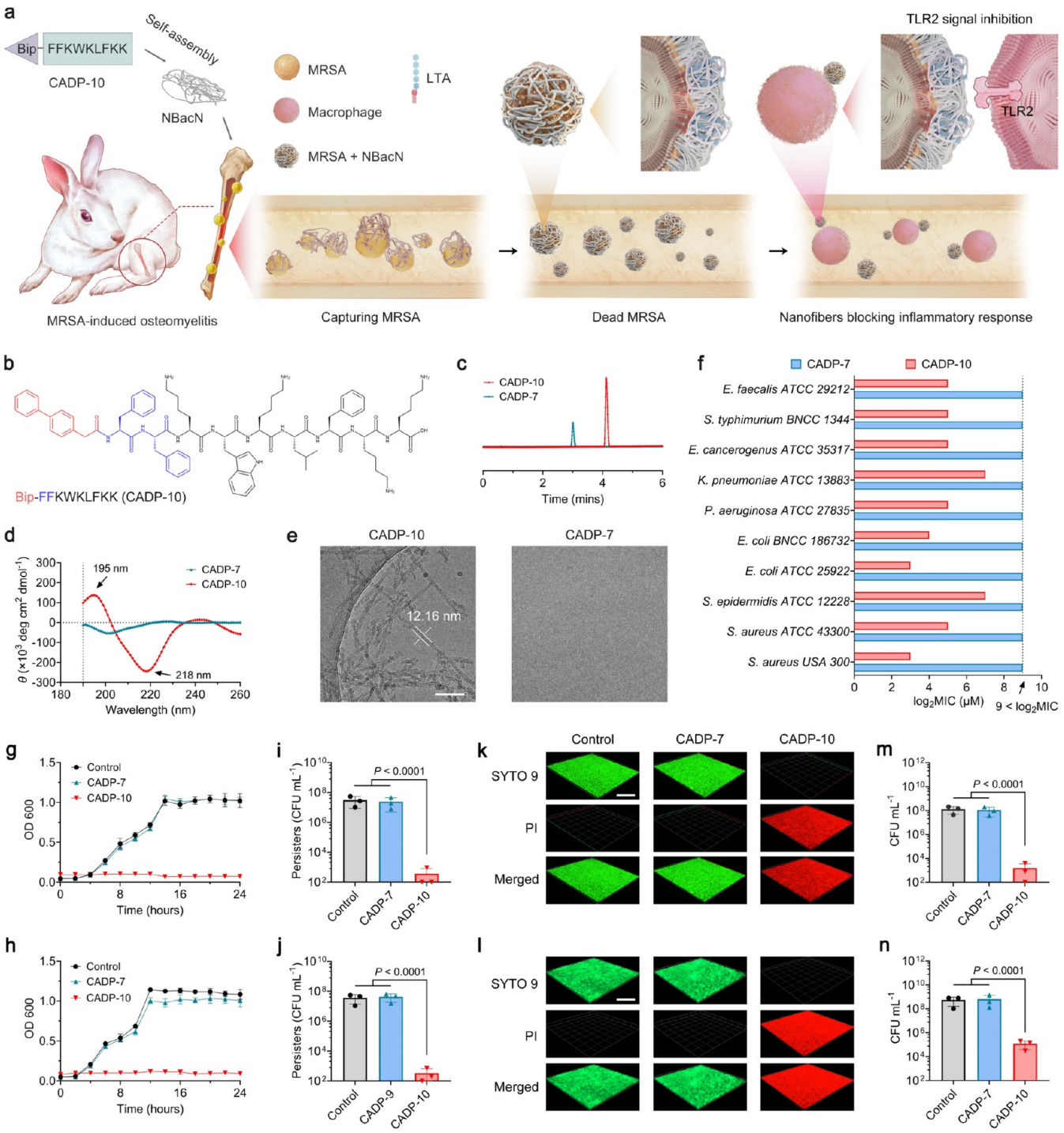

Figure 1. The molecular design of the CADP-10 and the bactericidal ability of CADP-10 *in vitro*. (a) The schematic illustration of the CADP-10 treatment of osteomyelitis for antibacterial while alleviating inflammation. (b) The molecular structure of CADP-10. (c) The LC spectra of CADP-7 and CADP-10. (d) The circular dichroism (CD) spectra of CADP-7 and CADP-10. (e) Cyro-electron microscopy (Cyro-EM) images of the CADP-7 and CADP-10. Scale bar, 100 nm. (f) The minimal inhibitory concentration (MIC) of CADP-7 and CADP-10 against broad-spectrum bacteria, respectively. (g) The growth curves of MRSA under the treatment of CADP-7 and CADP-10, respectively. The MRSA concentration at the starting point was 1×10^6 CFU mL^{-1}. Individual data are presented as mean ± s.d. (n = 3). (h) The growth curves of MRE under the treatment of CADP-7 and CADP-10, respectively. The MRE concentration at the starting point was 1×10^6 CFU mL^{-1}. Individual data are presented as mean ± s.d. (n = 3). (i) The anti-MRSA persister activity of CADP-7 and CADP-10, respectively. Individual data are presented as mean ± s.d. (n = 3). (j) The anti-MRE persister activity of CADP-7 and CADP-10, respectively. Individual data are presented as mean ± s.d. (n = 3). (k, l) The laser scanning confocal microscopy (LSCM) images of the treated MRSA-biofilm (k) or the treated MRE-biofilm (l) stained with SYTO 9 (live) and PI (dead), respectively. The bacterial biofilms were combined with CADP-7 and CADP-10, and coincubated for 2 h. Then, the treated biofilm was stained with SYTO 9 and PI. Scale bar, 160 μm. (m, n) The activity of CADP-7 and CADP-10 against biofilm-encased bacteria. MRSA (m) and MRE (n). The minimum detection of bacterial concentration was 100 CFU mL^{-1}. Individual data are presented as mean ± s.d. (n = 3). Statistical analysis in (i–n) was conducted using a two-tailed Student's t test.

https://doi.org/10.1021/acsnano.4c18858
ACS Nano XXXX, XXX, XXX−XXX

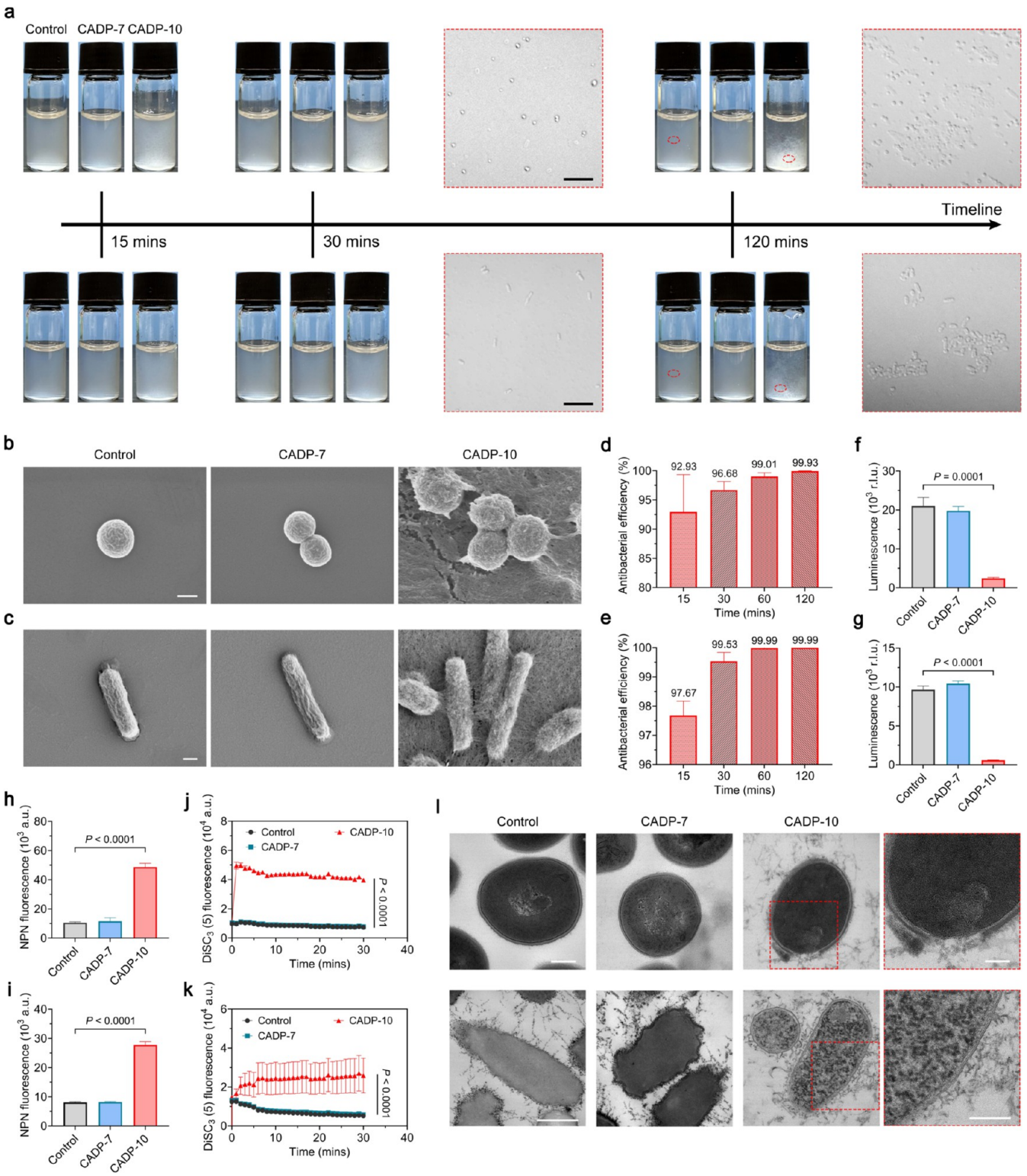

Figure 2. The mode of action in CADP-10 against bacteria. (a) The optical images of bacteria treated with CADP-7 and CADP-10 at 15, 30, and 120 min, respectively. MRSA was at the top, and MRE was at the bottom. Scale bar, 10 μm. Bacteria were combined with peptides in glass bottles and coincubated for 120 min. At 15, 30, and 120 min, respectively, take pictures of the glass bottles. (b, c) The field emission scanning electron microscope (FE-SEM) images of bacteria treated with CADP-7 and CADP-10. Scale bar in MRSA (b), 400 nm; Scale bar in MRE (c), 400 nm. (d) The antibacterial efficiency of CADP-10 against MRSA (5×10^8 CFU mL^{-1}) at 15, 30, 60, and 120 min. Individual data are presented as mean ± s.d. (n = 3). (e) The antibacterial efficiency of CADP-10 against MRE (1×10^8 CFU mL^{-1}) at 15, 30, 60, and 120 min. Individual data are presented as mean ± s.d. (n = 3). (f) Intracellular ATP levels in MRSA under the treatment of CADP-7 and CADP-10. Individual data are presented as mean ± s.d. (n = 3). (g) Intracellular ATP levels in MRE under the treatment of CADP-7 and CADP-10. Individual data are presented as mean ± s.d. (n = 3). (h, i) The NPN fluorescence intensity of bacterial suspension after the addition of CADP-7 and CADP-10. MRSA (h) and MRE (i). NPN was added to the bacterial suspension to indicate the changes in the membrane integrity. Higher fluorescence intensity meant more damage to the membrane. Individual data are presented as mean ± s.d. (n =

https://doi.org/10.1021/acsnano.4c18858
ACS Nano XXXX, XXX, XXX−XXX

Figure 2. continued

3). (j, k) 3,3-dipropylthiadicarbocyanine iodide DiSC3(5) fluorescence intensity of bacterial suspension after the addition of CADP-7 and CADP-10. MRSA (j) and MRE (k). DiSC3(5) was added to the bacterial suspension to indicate the changes in the membrane potential. A higher fluorescence intensity meant that the membrane was more depolarized. Individual data are presented as mean ± s.d. (n = 3). (l) The transmission electron microscopy (TEM) images of bacteria under the treatment of CADP-7 and CADP-10 showed the bacterial morphology. MRSA was on the top: the scale bar, 200 nm; the scale bar in the enlarged image, 100 nm. MRE was at the bottom: the scale bar, 500 nm; the scale bar in the enlarged image, 250 nm. Statistical analysis in (d−g), and (h−k) was conducted using a two-tailed Student's t test.

through self-assembly into fibrous nanostructures.[15] This trapping can effectively inhibit the migration of bacteria without killing the bacteria. The trapped bacteria are passed out of the body through the intestines or urethra without causing inflammation. Key components on the surface of bacteria, such as Lipopolysaccharide (LPS)[16] in Gram-negative bacteria and lipoteichoic acids (LTA)[17] in Gram-positive bacteria, play critical roles in bacterial survival and pathogenicity. While these endotoxins are essential for maintaining bacterial wall integrity, they also bind to Toll-like receptors (TLR) on immune cells, triggering robust inflammatory responses.[18,19] Targeting these endotoxins presents a dual opportunity: it can disrupt bacterial homeostasis, leading to bacterial death, and simultaneously inhibit their interaction with TLRs, thus preventing excessive inflammation.

In this study, we report the development of a Cecropin A-derived peptide, CADP-10, designed to target a broad spectrum of bacteria while alleviating inflammation (Figure 1a). CADP-10 self-assembles into nanobacterial net (NBacN) that effectively inhibits planktonic MRSA and multidrug-resistant *Escherichia coli* (MRE), including persisters and biofilm-forming bacteria. The peptide demonstrates a high affinity for LPS and LTA, with dissociation constants of 1.69×10^{-7} M and 6.69×10^{-7} M, respectively, enabling it to recognize, envelop, and trap bacteria. Upon interaction with bacterial membranes, CADP-10 nanofibers alter membrane potential and disrupt membrane integrity, leading to bacterial death. Importantly, these NbacN are bound to LPS and LTA from dead bacteria, preventing their engagement with TLR receptors and effectively blocking downstream inflammatory pathways. Our findings indicate that CADP-10 has favorable biocompatibility *in vitro* and *in vivo*, effectively eradicating MRSA-induced osteomyelitis and promoting bone tissue healing. This work highlights the potential of CADP-10 as a multifunctional therapeutic agent in the treatment of infectious inflammatory diseases.

RESULTS AND DISCUSSION

Design and Characterization of CADP-7 and CADP-10, and Their Antibacterial Activity *In Vitro*. CADP-10 comprised a hydrophobic motif (4-biphenyl acetic acid, Bip)[20] to ensure the system's membrane targeting ability, an assembly motif (FF)[21−24] to improve the self-assembly capability of peptides, and a cationic fragment (KWKLFKK) from Cecropin A (a host defense peptide)[25] to target negatively charged bacterial membranes (Figures 1b and S1). The Bip-FF motif was covalently bound to KWKLFKK (CADP-7), truncated from Cecropin A, which increased the hydrophobicity of CADP-7 (Figure 1c). Circular dichroism (CD) spectra indicated that CADP-7 did not exhibit a defined secondary structure (Figure 1d). In contrast, CADP-10 displayed a β-sheet structure, characterized by a positive peak at 195 nm and a negative peak at 218 nm, which facilitated its assembly into nanofibers. Subsequently, we employed a cryo-electron microscope to examine the morphology of CADP-7 and CADP-10 in phosphate buffer solution (PBS). CADP-7 did not form any observable structure, while CADP-10 successfully formed nanofibers (Figure 1e).

First, we evaluated the antibacterial capacity of CADP-7 and CADP-10 *in vitro*. The minimum inhibitory concentrations (MIC) of CADP-7 against various bacterial strains exceeded 512 μM, while the MIC of CADP-10 did not exceed 128 μM across different strains. These results indicated that CADP-10 exhibited broad-spectrum antibacterial activity, whereas CADP-7 showed no antibacterial effects (Figure 1f). To investigate the antibacterial activity of CADP-10, we selected a representative Gram-positive bacterium, methicillin-resistant *Staphylococcus aureus* USA 300 (MRSA), and a representative Gram-negative bacterium, multidrug-resistant *Escherichia coli* BNCC 186732 (MRE). The minimum bactericidal concentrations of CADP-10 against MRSA and MRE were 8 μM and 16 μM, respectively. We monitored the growth curves of the bacteria in the presence of CADP-7 and CADP-10 (Figure 1g,1h). The growth curve for the CADP-7 group increased over time, showing no significant difference compared to the Control group. In contrast, the growth curve for the CADP-10 group remained stable and did not increase over time, indicating that CADP-10 possessed strong bacteriostatic capabilities. After 8 h of coculture with the peptides (Figure S2a,b), the MRSA concentration in the CADP-10 group decreased by approximately 10^5 times compared to the control group. Similarly, the MRE concentration in the CADP-10 group dropped by about 10^7 times compared to the control group. These results demonstrated that CADP-10 could significantly inhibit bacterial growth.

Bacterial persisters and biofilms are significant contributors to infection recurrence and antibiotic resistance.[26,27] We coincubated CADP-10 with bacterial persisters for 2 h (Figure 1i,1j). Compared to the control group, the concentration of MRSA persisters in the CADP-10 group decreased by approximately 10^5 times. Similarly, the concentration of MRE persisters also decreased by about 10^5 times in the CADP-10 group. Next, we assessed whether CADP-10 could effectively kill and eradicate established biofilms. Live/dead fluorescent assays revealed that PI entered bacteria in the CADP-10 group (Figure 1k,1l). This could be attributed to CADP-10 killing bacteria, thereby increasing the membrane permeability and allowing PI to enter the bacteria. Alternatively, it might also be due to the permeation effect of CADP-10, which promoted the entry of PI into live bacteria. To further verify the antibacterial activity of CADP-10 on bacterial biofilms, the spread plate method was used to evaluate whether biofilm-encased bacteria from different treatment groups were alive or dead. CADP-10 eliminated 99.99% of biofilm-encased MRSA and 99.97% of biofilm-

https://doi.org/10.1021/acsnano.4c18858
ACS Nano XXXX, XXX, XXX−XXX

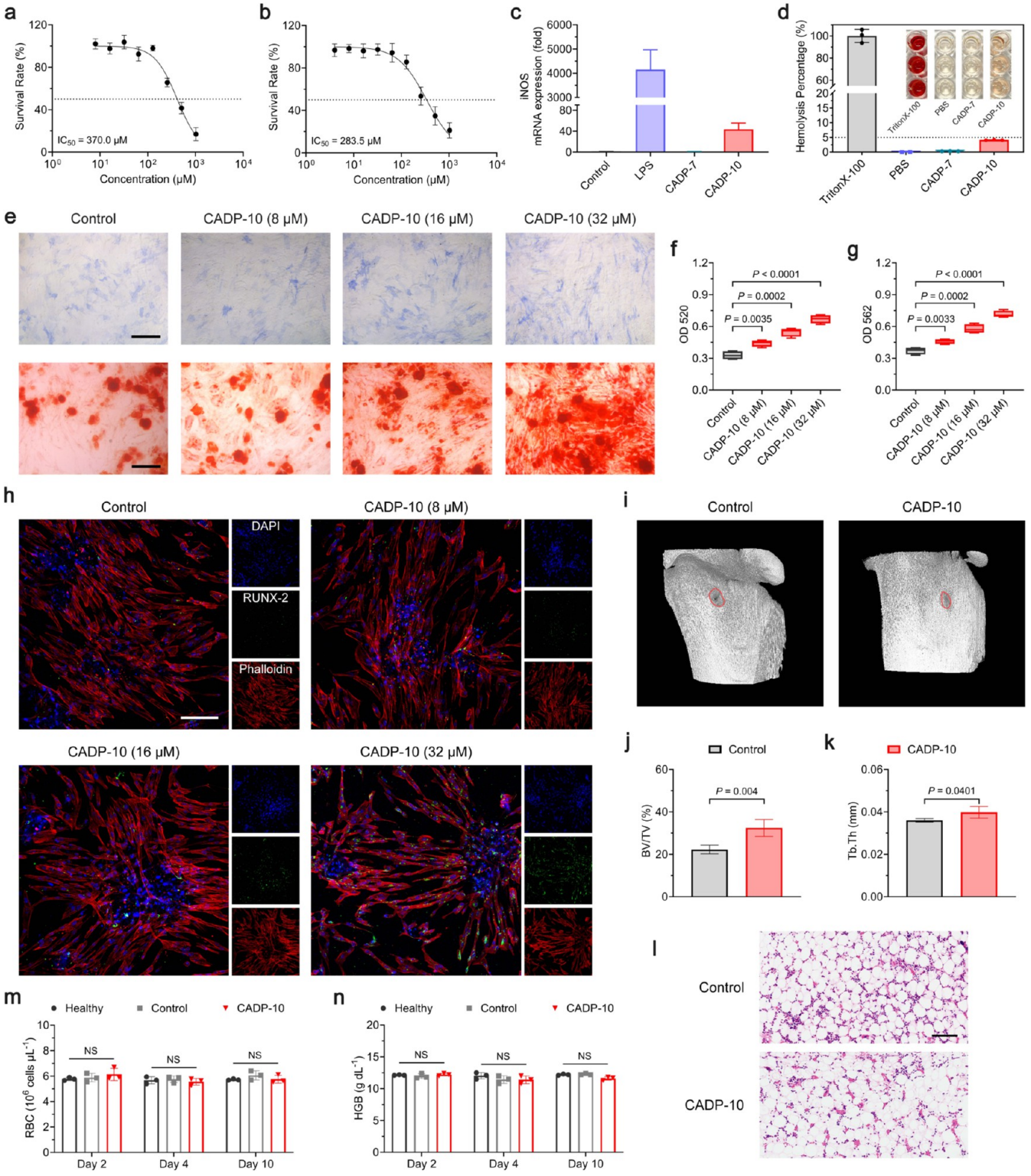

Figure 3. The biosafety of CADP-10 *in vitro* and the osteogenic activity of CADP-10 *in vitro*. (a) The survival rate of human bone mesenchymal stem cells (hBMSC) treated with CADP-10 at different concentrations. Individual data are presented as mean ± s.d. (n = 3). (b) The survival rate of bone marrow-derived macrophages (BMDMs) treated with CADP-10 at different concentrations. Individual data are presented as mean ± s.d. (n = 3). (c) qPCR quantification of iNOS mRNA expression in the BMDMs under the treatment of LPS (positive control for M1 polarization), CADP-7, and CADP-10, respectively. Individual data are presented as mean ± s.d. (n = 3). (d) The hemolysis percentage of rabbit red blood cells (rRBC) under the treatment of CADP-7 (320 μM), CADP-10 (320 μM), and tritonX-100 (positive control), respectively. Individual data are presented as mean ± s.d. (n = 3). (e) ALP staining images (on the top) and alizarin red S (ARS) images (at the bottom) of hBMSC in the cultures containing CADP-10 at the concentration of 8 μM, 16 μM, and 32 μM, respectively. Scale bar, 200 μm. (f) The quantification of ALP staining in e. Individual data are presented as mean ± s.d. (n = 3). (g) The quantification of ARS staining in e. Individual data are presented as mean ± s.d. (n = 3). (h) RUNX-2 immunofluorescence staining (green) images of hBMSC in the osteogenic culture medium containing CADP-10 at the concentration of 8 μM, 16 μM, and 32 μM, respectively. The nucleus was stained

https://doi.org/10.1021/acsnano.4c18858
ACS Nano XXXX, XXX, XXX−XXX

Figure 3. continued

with DAPI (blue) and the cell skeleton was stained red. Scale bar, 100 μm. (i) The microcomputed tomography (micro-CT) images of the rabbit tibias treated with CADP-10. (j) The bone-volume fraction (BV/TV) analysis based on the micro-CT tomography images on day 10. Individual data are presented as mean ± s.d. (n = 3). (k) The trabecular thickness (Tb. Th) analysis based on the micro-CT tomography images. Individual data are presented as mean ± s.d. (n = 3). (l) H&E staining images of the mouse tibias. (m, n) The red blood cells (RBC) count (m) and hemoglobin (HGB) concentration (n) in whole blood of rabbits receiving the CADP-10 treatment. Individual data are presented as mean ± s.d. (n = 3).

encased MRE (Figure 1m,1n). The biofilm mass treated with CADP-10 was stained with crystal violet. CADP-10 reduced the MRSA biofilm mass by 53.63% and the MRE biofilm mass by 55.78% (Figure S2c,d). These results demonstrate that CADP-10 effectively eradicates bacterial biofilms.

Interaction between CADP-10 and Bacteria and Its Rapid Antibacterial Ability *In Vitro*. To better observe the interaction between CADP-10 and bacteria, we mixed the two and placed them in a glass bottle, monitoring the changes in the bacterial suspension over time (Figure 2a). CADP-10 enveloped the bacteria, gradually aggregating and eventually precipitating in the bottle. Optical images indicated that, compared to the Control group, CADP-10 facilitated bacterial accumulation. Next, we assessed the surface zeta potential of the bacteria (Figure S3a). CADP-10 was positively charged, and upon contact, it altered the bacteria's surface zeta potential from negative to positive, demonstrating an electrostatic interaction between CADP-10 and the bacteria. Using field emission scanning electron microscopy (FE-SEM), we examined the morphology of bacteria treated with CADP-10 (Figure 2b,2c). The FE-SEM images revealed that dense CADP-10 nanofibers completely covered the bacteria, causing them to aggregate. These findings confirmed that CADP-10 enveloped and bound the bacteria together. Furthermore, CADP-10 was shown to kill 92.93% of MRSA and 97.67% of MRE within 15 min (Figures 2d,2e, and S3b,c). After 30 min, it killed 96.68% of MRSA and 99.53% of MRE. Ultimately, at 120 min, CADP-10 eradicated nearly all MRSA (99.93%) and MRE (99.99%). These results suggest that CADP-10 effectively kills bacteria while encasing them.

To further understand how CADP-10 killed bacteria, we cocultured the bacteria with CADP-10 for 2 h. Compared to the Control group, intracellular ATP levels in the CADP-10 group significantly decreased (Figure 2f,2g), indicating a substantial inhibition of bacterial metabolism. We then evaluated membrane permeability and membrane potential under CADP-10 treatment. *N*-phenyl-1-naphthylamine (NPN),[28] a fluorescent indicator, was used to assess changes in membrane permeability (Figure 2h,2i). The NPN fluorescent intensity in the CADP-10 group was significantly higher than in the control group, suggesting that CADP-10 altered bacterial membrane permeability. Additionally, 3,3-dipropylthiadicarbocyanine iodide ($DiSC_3(5)$),[29] a membrane depolarized probe, to indicate changes in membrane potential due to membrane damage (Figure 2j,2k). After the addition of CADP-10, the fluorescence intensity of $DiSC_3(5)$ in the CADP-10 group increased rapidly and stabilized over time. These results indicated that CADP-10 depolarized and damaged the bacterial membrane. Transmission electron microscopy (TEM) images further confirmed that CADP-10 destroyed the bacterial membrane (Figure 2l). Moreover, CADP-10 also induced the production and aggregation of reactive oxygen species (ROS) in bacteria (Figure S4),[30,31] disrupting bacterial homeostasis and exacerbating membrane damage.

Biosafety and Osteogenic Activity of CADP-10 *In Vitro*. To evaluate the toxicity of CADP-10 *in vitro*, we used human bone mesenchymal stem cells (hBMSCs) and bone marrow-derived macrophages (BMDMs) (Figure 3a,3b). The cells were incubated with CADP-10 for 24 h, revealing half maximal inhibitory concentrations (IC_{50}) of 370.0 μM for hBMSCs and 283.5 μM for BMDMs, respectively. Additionally, CADP-10 had no effect on BMDM polarization (Figures 3c and S5). A hemolysis test showed that at a concentration of 320 μM, which is 40 times higher than the MIC for both MRSA and MRE, the hemolysis percentage of rabbit red blood cells (RBC) was less than 5% (Figure 3d). These results indicate that CADP-10 has good biocompatibility.

Next, we evaluated the osteoinductive activity of CADP-10 *in vitro* using hBMSCs. We conducted alkaline phosphatase (ALP)[32] and alizarin red S staining (Figure 3e)[33] after culturing the hBMSCs with CADP-10 at 8 μM, 16 μM, and 32 μM for 7 and 21 days, respectively. After 7 days, ALP expression in hBMSCs was significantly upregulated with CADP-10 treatment (Figure 3f). After 21 days, substantial mineral nodules formed in the CADP-10 group (Figure 3g). Immunofluorescence staining showed that the expression of RUNX-2 protein in the CADP-10 group was significantly increased compared to the control group (Figure 3h and Figure S6a). RUNX-2 protein accumulated in the nucleus of cells in the CADP-10 group, indicating an active state. These results demonstrate that CADP-10 can induce osteogenic differentiation of hBMSCs *in vitro*.

To evaluate the osteogenic activity and biosafety of CADP-10 *in vivo*, we implanted nanofibers into tibial bone defects in rabbits and observed bone formation. After 10 days, the micro-CT was used to investigate the statement of rabbit tibia healing (Figure 3i).[34] In the Control group, bone tissue defects were still evident, whereas in the CADP-10 group, new bone had fully formed in the defect. The percent bone volume (BV/TV) in the Control group was approximately 20% (Figure 3j). After CADP-10 treatment, BV/TV increased to about 30%. Additionally, the thickness (Tb. Th) in the CADP-10 group was significantly greater than in the Control group (Figure 3k), while trabecular separation (Tb. Sp) was lower in the CADP-10 group compared to the Control group (Figure S6b). These results indicate that CADP-10 promotes bone formation *in vivo*.

Histological examination (HE staining) of the CADP-10 group revealed no abnormal signs (Figure 3l). We also conducted blood routine tests on whole blood from rabbits in both groups on days 2, 4, and 10. Compared to the healthy group, there were no abnormalities in the red blood cell (RBC) count and the concentration of hemoglobin (HGB) in the CADP-10 group, indicating no hemolysis (Figures 3m and 3n). Additionally, platelet (PLT) and white blood cell (WBC) counts showed no abnormalities (Figure S7a,b), suggesting

https://doi.org/10.1021/acsnano.4c18858
ACS Nano XXXX, XXX, XXX−XXX

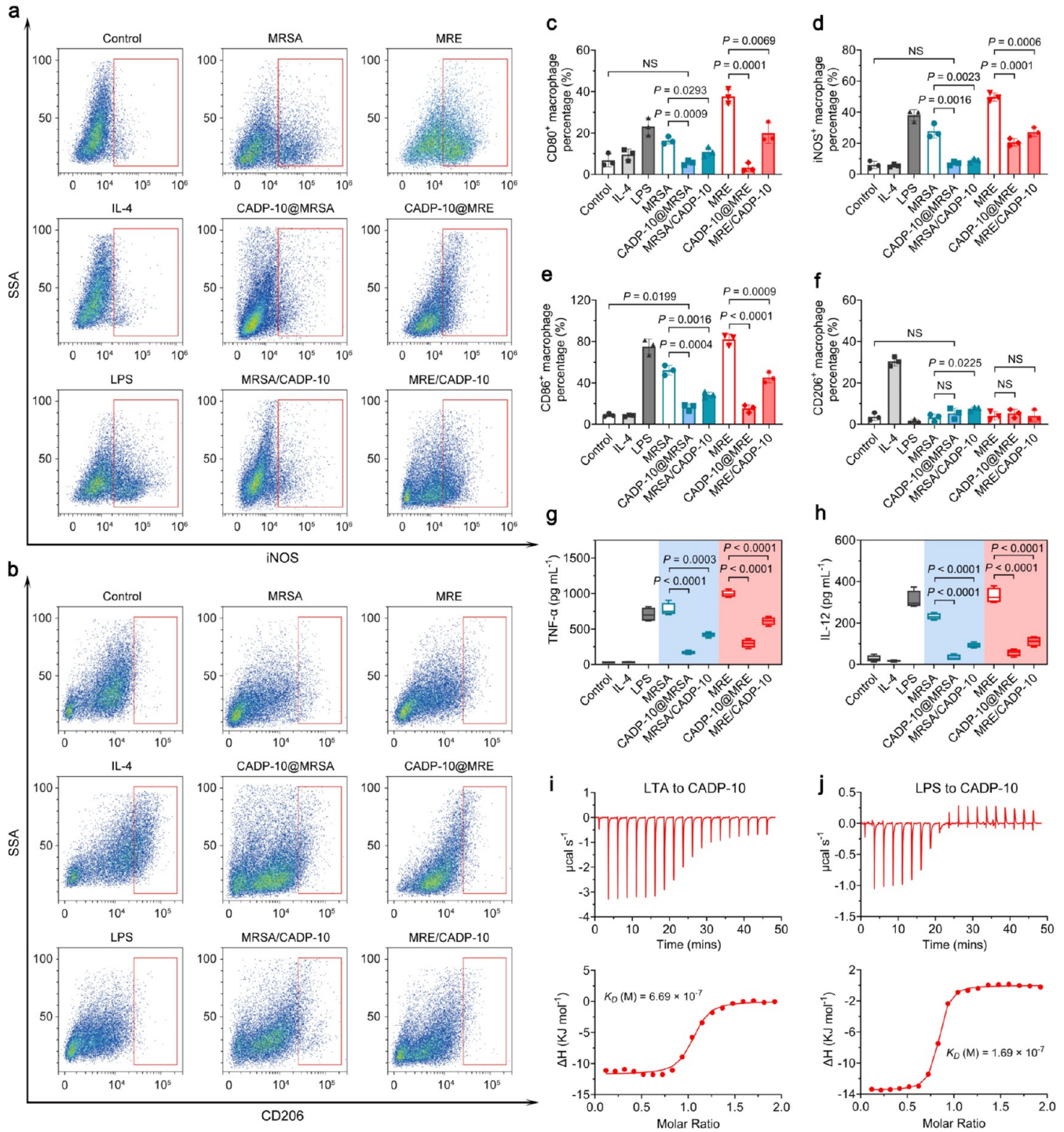

Figure 4. The passive anti-inflammatory study of CADP-10 *in vitro*. (a, b) The flow cytometry analysis of iNOS$^+$ macrophages (a) and CD206$^+$ macrophages (b) in the total macrophages under the treatment of different conditions. For the CADP-10@bacteria group, CADP-10 and bacteria were added to the medium and coincubated for 30 min, and the medium was added to wells in the corresponding plates containing adherent BMDMs. These plates were placed in an incubator at 37 °C for 24 h. For the bacteria/CADP-10 group, the medium containing bacteria was added to the wells in the corresponding plates containing adherent BMDMs and coincubated for 12 h. Next, the CADP-10 (final concentration: 128 μM) was added to these plates, mixed, and coincubated for another 12 h. (c–f) The percentage of CD80$^+$ macrophages (c), iNOS$^+$ macrophages (d), CD86$^+$ macrophages (e), and CD206$^+$ macrophages (f) in the total macrophages under the treatment of different conditions. Individual data are presented as mean ± s.d. (n = 3). (g, h) The concentration of TNF-α (g) and IL-12 (h) secreted by BMDMs under the treatment of different conditions. Individual data are presented as mean ± s.d. (n = 3). (i) The affinity between lipoteichoic acid (LTA) and CADP-10. The dissociation constant of CADP-10 for LTA was 6.69 × 10^{-7} M. (j) The affinity between lipopolysaccharide (LPS) and CADP-10. The dissociation constant of CADP-10 for LPS was 1.69 × 10^{-7} M. Statistical analysis in c-h was conducted using a two-tailed Student's t test.

https://doi.org/10.1021/acsnano.4c18858
ACS Nano XXXX, XXX, XXX−XXX

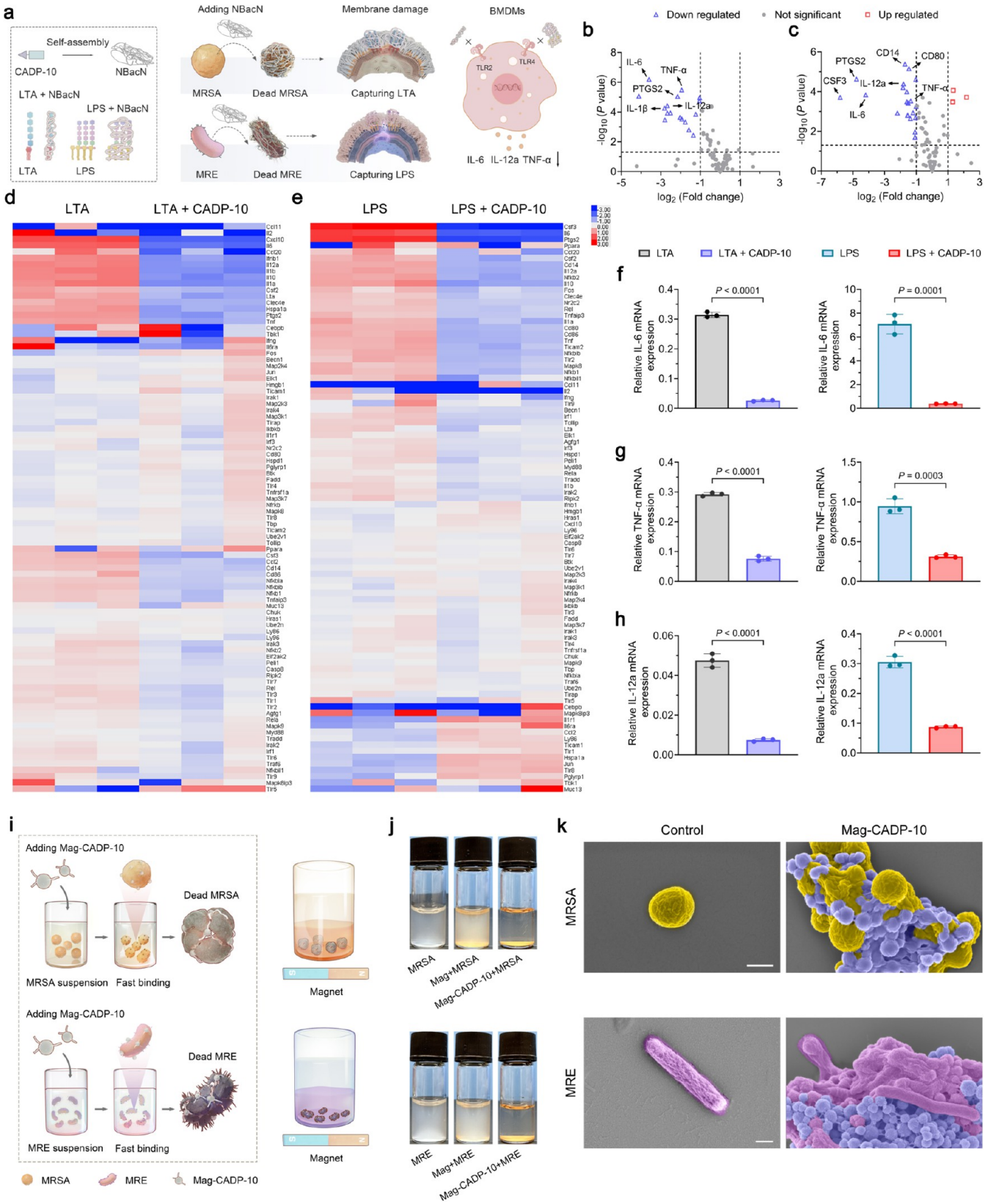

Figure 5. CADP-10 inhibited LTA- or LPS-induced inflammation in BMDMs. (a) Schematic illustration of the mechanism by which CADP-10 inhibited LTA- or LPS-induced inflammation. (b) Volcano plot showed that the down regulated and the up regulated mRNA of MRSA treated with LTA or LTA + CADP-10. (c) Volcano plot showed that the down regulated and the up regulated mRNA of MRSA treated with LPS or LPS + CADP-10. (d) mRNA heatmap of Toll-like receptor signaling pathway related mRNA expression in BMDMs stimulated with LTA or LTA + CADP-10. (e) mRNA heatmap of Toll-like receptor signaling pathway-related mRNA expression in BMDMs stimulated with LPS or LPS + CADP-10. (f) The relative IL-6 mRNA expression in BMDMs treated with LTA, LTA + CADP-10, LPS, and LPS + CADP-10, respectively. (g) The relative TNF-α mRNA expression in BMDMs treated with LTA, LTA + CADP-10, LPS, and LPS + CADP-10,

https://doi.org/10.1021/acsnano.4c18858
ACS Nano XXXX, XXX, XXX−XXX

Figure 5. continued

respectively. (h) The relative IL-12a mRNA expression in BMDMs treated with LTA, LTA + CADP-10, LPS, and LPS + CADP-10, respectively. (i) Schematic illustration of the Mag-CADP-10 capturing bacteria. (j) Optical images of bacteria under the treatment of Mag and Mag-CADP-10, respectively. (k) The FE-SEM images of Mag-CADP-10 binding to MRSA and MRE, respectively. Scale bar in the MRSA image, 500 nm; Scale bar in the MRE image, 500 nm.

that CADP-10 does not induce clotting toxicity or inflammation. Overall, these results demonstrate that CADP-10 possesses excellent biocompatibility, ensuring its anti-infectious activity without side effects.

CADP-10 Suppressed Bacteria-Induced Inflammation by Targeting LTA or LPS *In Vitro*. First, we tested whether CADP-10 could inhibit the bacteria-induced polarization of the bone marrow-derived macrophages (BMDMs) toward M1 phenotype (pro-inflammatory).[35] BMDMs were extracted from mice and cultured in DMEM, then seeded in 24-well plates. The BMDMs were stimulated with bacteria (MRSA or MRE), IL-4 (anti-inflammatory positive control), LPS (pro-inflammatory positive control), CADP-10@bacteria, and bacteria/CADP-10. The treated BMDMs were labeled with pro-inflammatory antibodies (CD80, iNOS, and CD86) as well as an anti-inflammatory antibody (CD206), followed by flow cytometric analyses (Figures 4a,4b, and S8). When bacteria were directly added to the BMDMs, the percentages of $CD86^+$, $CD80^+$, and $iNOS^+$ macrophages increased significantly (Figure 4c−4f). However, when CADP-10 was combined with the bacteria, the percentages of $CD86^+$, $CD80^+$, and $iNOS^+$ macrophages in the CADP-10@bacteria group significantly decreased compared to the bacteria-only group. Furthermore, there were no significant differences in the percentages of $CD86^+$, $CD80^+$, and $iNOS^+$ macrophages between the CADP-10@bacteria group and the control group. To further examine the effects of CADP-10 on inflammation, we first added bacteria to the BMDMs and cultured them for 12 h. We then introduced CADP-10 and continued culturing for another 12 h. Compared to the bacteria group, the percentages of $CD86^+$, $CD80^+$, and $iNOS^+$ macrophages in the CADP-10/bacteria group were significantly lower. The percentage of $CD206^+$ macrophages in all groups did not change compared to the control group. These results demonstrate that CADP-10 can block M1 polarization in BMDMs treated with bacteria. We also measured the cytokines secreted by macrophages using enzyme-linked immunosorbent assay (ELISA). Consistent with the flow cytometric analyses, the concentrations of pro-inflammatory factors (TNF-α, IL-12, and IL-6) in the CADP-10@bacteria and bacteria/CADP-10 groups were significantly reduced compared to the bacteria group and the LPS group (Figures 4g,4h, and S9a). These results indicated that CADP-10 covering bacterial surfaces prevented the binding of LPS/LTA to TLR receptors, blocking downstream inflammatory pathways and leading to a decline in proinflammatory cytokines. CADP-10 effectively decreases the expression of pro-inflammatory factors in macrophages.

LPS (from Gram-negative *E. coli*) and LTA (from Gram-positive *S. aureus*) are key antigens present on the bacterial surface. Based on SEM results, CADP-10 can coat the surface of bacteria, leading us to hypothesize that CADP-10 binds to these antigens, preventing them from interacting with Toll-like receptors (TLRs). We assessed the binding affinity of CADP-10 to these antigens using isothermal titration calorimetry (ITC).[36] The dissociation constant of CADP-10 for LTA was found to be 6.69×10^{-7} M (Figure 4i), while the dissociation constant of CADP-10 for LPS was 1.69×10^{-7} M (Figure 4j). These results indicated a high affinity of CADP-10 for both LPS and LTA.

To further evaluate whether targeting LPS and LTA could decrease inflammatory cytokine levels, we mixed LPS and LTA with BMDMs and subsequently added CADP-10. Changes in related gene expression were analyzed using the Quantitative Real-time PCR (qPCR) system. As shown in Figure 5a, CADP-10 effectively recognized and bound free LPS and LTA, preventing their interaction with TLRs on BMDMs and thereby blocking the inflammatory response. The mRNA volcano plot (Figures 5b and 5c) and heatmap (Figures 5d and 5e) of the TLR signaling pathway revealed that, compared to the endotoxin (LPS or LTA) group, the expression of inflammation-related mRNAs, including IL-6 (Figure 5f), TNF-α (Figure 5g), and IL-12a (Figure 5h), was significantly reduced in the endotoxin (LPS or LTA) + CADP-10 group. These findings confirmed that CADP-10 interacted with LPS and LTA, preventing their engagement with TLR receptors and effectively blocking downstream inflammatory pathways.

To further verify the strong affinity of CADP-10 for bacterial surfaces, we attached CADP-10 to magnetic beads and utilized them to capture bacteria (Figure 5i and Video Clips S1−S4). Under magnetic force, these modified beads effectively dragged all bacteria to the bottom of a glass bottle in less than a minute (Figure 5j). The supernatant in the Mag-CADP-10 + bacteria group appeared clear. After the magnetic beads captured the bacteria, we measured the optical density at 600 nm (OD_{600}) of the supernatant (Figure S9b). The OD_{600} values in the Mag-CADP-10 + bacteria group were significantly lower compared to the bacteria and Mag + bacteria groups. Moreover, we used field emission scanning electron microscopy (FE-SEM) to observe the morphology of bacteria treated with Mag-CADP-10 (Figure 5k). The FE-SEM images demonstrated that Mag-CADP-10 adhered tightly to the bacterial surface, further supporting the strong binding affinity of CADP-10 to bacterial antigens.

Therapeutic Ability of CADP-10 on MRSA-Infected Osteomyelitis in Rabbits. Before using CADP-10 to treat osteomyelitis in rabbits, we evaluated its antimicrobial activity in a simulated bone marrow cavity environment *in vitro*. Bone marrow was extracted from rabbit tibias and homogenized (Figure S10a). We added CADP-10 to the homogenate containing MRSA and cultured it for different durations. After 1 h, the MRSA counts in the CADP-10 (128 μM) group decreased by about 5 times compared to the Control group. After 4 h, the MRSA counts in the CADP-10 (128 μM) group decreased by about 35 times compared to the Control group. These results indicate that CADP-10 exhibits potent antibacterial activity in a simulated bone marrow cavity environment. In contrast to CADP-10, commercial antibiotics often lead to bacterial resistance, shortening their useful life.[37] For instance, MRSA began to develop resistance to gentamicin (Gen) by the sixth generation (Figure S10b). By the 30th generation, the MIC of gentamicin against MRSA had

https://doi.org/10.1021/acsnano.4c18858
ACS Nano XXXX, XXX, XXX−XXX

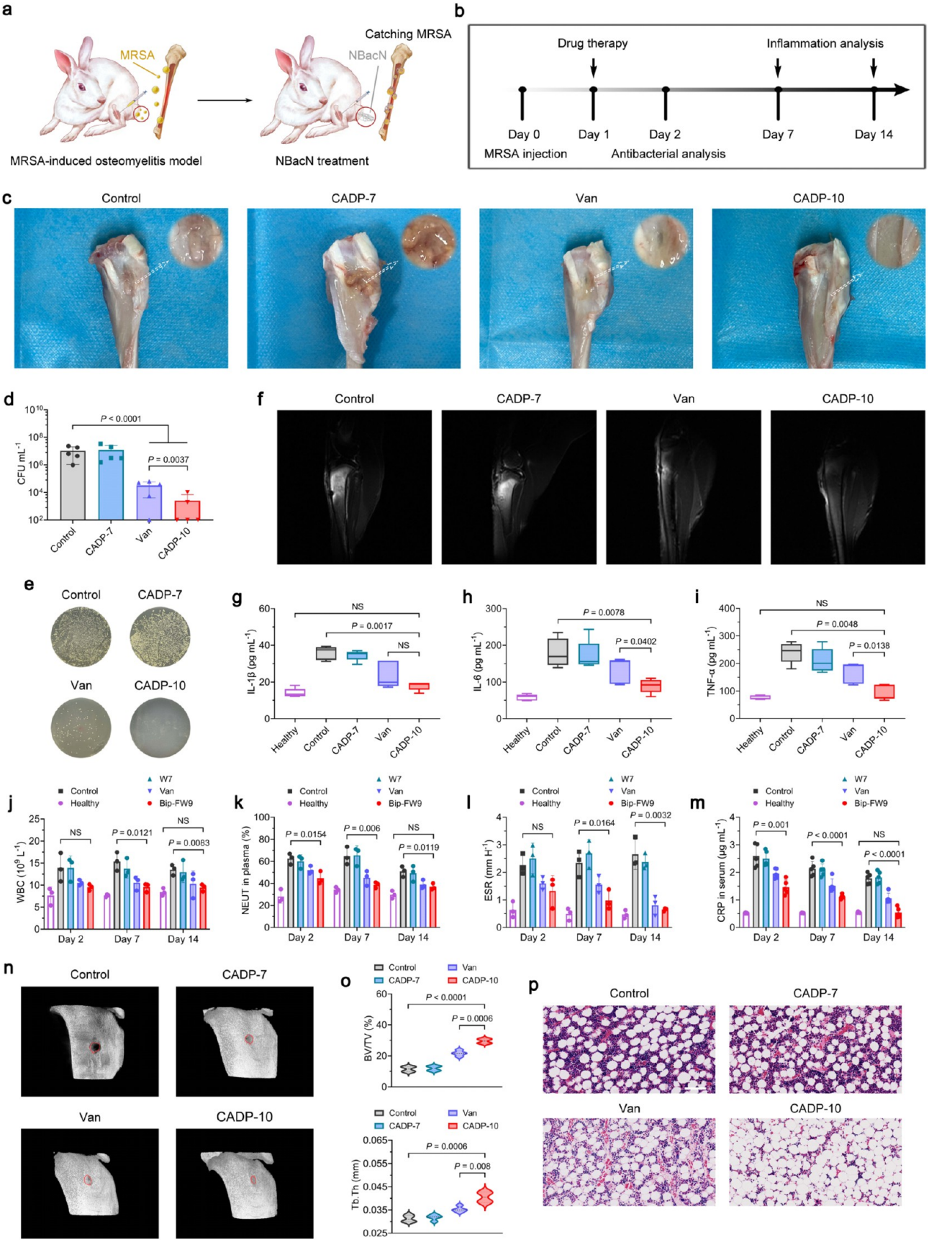

Figure 6. | The antibacterial ability of CADP-10 on the MRSA-infected rabbit osteomyelitis model *in vivo*. (a) Schematic diagram of establishment and treatment of osteomyelitis in rabbits. (b) The timeline for rabbit experiments *in vivo*. On day 0, rabbits were infected with MRSA by injecting MRSA into the tibial cavity; on day 1, rabbits infected with MRSA were treated by injecting vancomycin (Van) and CADP-10 into the tibial cavity; on day 2, the bone marrow fluid from the tibial cavity in each group was extracted for antibacterial analysis;

https://doi.org/10.1021/acsnano.4c18858
ACS Nano XXXX, XXX, XXX−XXX

Figure 6. continued

on day 7 and day 14, the inflammation analysis in the rabbits infected with MRSA was measured after the treatment. (c) The optical images of the tibias from the rabbits infected with MRSA after the treatment of CADP-7, vancomycin (Van), and CADP-10 on day 10. The infected tissue was indicated and magnified in the images. (d) The MRSA quantification in the tibias of the rabbits with MRSA on the day after the treatment. Individual data are presented as mean ± s.d. (n = 5). (e) The representative bacterial LB agar plates from the corresponding group in d for directly showing that CADP-10 had greater bactericidal power than the other two groups. (f) The magnetic resonance images of the tibias from the rabbits infected with MRSA after the treatment of CADP-7, vancomycin (Van), and CADP-10 on day 10. (g–i), The concentration of proinflammatory cytokines in serum from the rabbits infected with MRSA in all groups on day 14. IL-1β (g), IL-6 (h), and TNF-α (i). Individual data are presented as mean ± s.d. (n = 5). (j–m) The white blood cell count (j), neutrophil percentage (k), erythrocyte sedimentation rate (l), and C-reactive protein (m) in peripheral blood from the rabbits infected with MRSA in all groups on day 2, day 7, and day 14, respectively. NEUT, neutrophils (n = 3); ESR, erythrocyte sedimentation rate (n = 3); WBC, white blood cells (n = 3); CRP, C-reactive protein (n = 5). (n) The microcomputed tomography (micro-CT) images of the tibias in rabbits infected with MRSA in all groups on day 14. (o) The bone-volume fraction (BV/TV) analysis and trabecular thickness (Tb. Th) analysis based on the Micro-CT tomography images in all groups. Individual data are presented as mean ± s.d. (n = 3). (p) H&E staining images of bone marrow tissues from rabbits infected with MRSA in all groups on day 14. Scale bar, 100 μm.

increased 128-fold. Notably, MRSA did not develop resistance to CADP-10.

Next, we investigated the antibacterial activity of CADP-10 in a rabbit osteomyelitis model.[38] The experimental timeline is illustrated in Figures 6a,6b. Rabbits in the Control and CADP-7 groups exhibited evident pus and ulceration in the tibia (Figure 6c), indicating severe bacterial infections. In contrast, after treatment with vancomycin (Van) and CADP-10, the tibias showed no pus, ulceration, or apparent signs of infection. While the Van group displayed significant defects, the CADP-10 group exhibited signs of healing. We measured bacterial concentration in the bone marrow cavity of all groups on day 2 (Figure 6d,6e). Following treatment with vancomycin and CADP-10, bacterial concentrations decreased significantly. Compared to the control group, the bacterial concentration in the CADP-10 group decreased by approximately 5,000 times (P < 0.0001). Additionally, when compared to the Van group, the bacterial concentration in the CADP-10 group was lower by about 10 times (P = 0.0037). Magnetic resonance imaging (MRI) further confirmed the results: the Control and CADP-7 groups showed high signs of infection, the Van group exhibited weak signs, while the CADP-10 group displayed no typical signs of infection (Figure 6f). These findings demonstrate that CADP-10 effectively eradicates bacteria *in vivo*, highlighting its therapeutic potential against MRSA-infected osteomyelitis. On day 7, serum was collected from rabbits in all groups (Figures 6g-6i). The levels of pro-inflammatory cytokines (IL-1β, IL-6, and TNF-α) in the CADP-10 group were significantly lower than those in the Control group, indicating a rapid recovery of the MRSA-infected rabbits treated with CADP-10. We also analyzed whole blood from the rabbits on days 2, 7, and 14. On day 2, the white blood cell (WBC) concentration and neutrophil (NEUT) percentage in the CADP-10 group were lower than in the Control group (Figure 6j,6k). By day 14, there were no significant differences in WBC concentration and NEUT percentage between the CADP-10 and healthy groups. Similar trends were observed in C-reactive protein (CRP) and erythrocyte sedimentation rate (ESR) levels (Figure 6l,6m), suggesting that CADP-10 treatment led to a gradual reduction in inflammation and facilitated recovery in MRSA-infected rabbits.

On day 10, micro-CT imaging was employed to assess the healing status of infected rabbit tibias across all groups (Figure 6n). In the Control and CADP-7 groups, bone tissue defects remained visible on day 14, while new bone formation was observed in the CADP-10 and Van groups. The bone volume/total volume ratio (BV/TV) in the CADP-10 group reached approximately 30% (Figure 6o), significantly higher than that in the Control group (P < 0.0001) and the Van group (P = 0.0006). Additionally, trabecular thickness (Tb. Th) values in the CADP-10 group were greater than those in the control (P = 0.0006) and Van groups (P = 0.008), indicating that CADP-10 promotes bone formation.

Histological examination (HE staining) on day 14 revealed numerous inflammatory cells in the bone marrow cavities of rabbits in the Control and CADP-7 groups, while inflammatory cell counts were significantly reduced in the CADP-10 group (Figure 6p). Furthermore, routine blood tests indicated that CADP-10 did not cause hemolysis or coagulation dysfunction (Figure S11). These findings collectively demonstrate that CADP-10 effectively eradicates infections and promotes bone tissue healing without adverse side effects, highlighting its potential as a therapeutic agent for osteomyelitis treatment.

CONCLUSIONS

We report the antimicrobial peptide CADP-10 as an effective agent against a broad spectrum of bacteria while simultaneously alleviating inflammatory responses. CADP-10 demonstrated potent activity against planktonic bacteria, persisters, and biofilms, showcasing its versatility in combating bacterial infections. The peptide self-assembles into nanofibers that can accurately recognize and rapidly bind to bacterial surfaces by targeting lipopolysaccharides (LPS) and lipoteichoic acid (LTA) found in the bacterial cell wall. Upon binding, CADP-10 induces significant alterations in bacterial membrane permeability and depolarizes the membrane potential, ultimately leading to membrane dysfunction and bacterial cell death. Notably, even after killing the bacteria, CADP-10 remains associated with LPS and LTA, effectively preventing these endotoxins from interacting with Toll-like receptors (TLRs) and thereby blocking the downstream inflammatory response. In terms of biosafety, CADP-10 exhibited favorable profiles in both *in vitro* and *in vivo* evaluations. *In vivo* experiments demonstrated that CADP-10 could rapidly eliminate osteomyelitis infections in rabbits while mitigating bacteria-induced inflammation. This dual action not only facilitated tissue repair in the infected rabbit tibia but also promoted a swift recovery, allowing the animals to return to health more quickly. Moreover, we acknowledge that during the treatment of osteomyelitis in rabbits, CADP-10 nanofibers may block small capillaries, thereby posing a risk of embolism.

Overall, this work highlights the potential of CADP-10 as a promising antimicrobial agent capable of effectively eliminating

https://doi.org/10.1021/acsnano.4c18858
ACS Nano XXXX, XXX, XXX–XXX

bacterial infections and addressing endotoxin-induced inflammation. The findings still underscore CADP-10s applicability in clinical settings for treating severe infections, particularly those complicated by persistent biofilms and inflammatory responses.

MATERIALS AND METHODS

Materials. Bip-FFKWKLFKK (CADP-10) and KWKLFKK (CADP-7) were synthesized by the GL Biochem (Shanghai, China). Rhodamine 6G, crystal violet, and rifampicin were purchased from Merck KGaA. *N*-phenyl-1-naphthylamine (NPN), 2.5% glutaraldehyde, and 3,3′-dipropylthiadicarbocyanine iodide (DiSC3(5)) were purchased from Aladdin. Lipopolysaccharides (LPS) from *E. coli* and lipoteichoic acid from *S. aureus* were purchased from Merck KGaA. Vancomycin (Van) and gentamicin (Gen) were purchased from Shanghai Macklin Biochemical Technology Co., Ltd. BeyomagTM Carboxyl Magnetic beads (200 nm) were purchased from Beyotime Biotechnology. (7Azabenzotriazol1yl)-N,N,N,N′-tetramethyluronium hexafluorophosphate (HBTU) was purchased from GL Biochem (Shanghai, China).

Circular Dichroism (CD) Spectra of CADP-10 and CADP-7. CADP-10 and CADP-7 were dissolved in deionized water (pH = 7.4) at a final concentration of 64 μM. Then, the peptide solutions were added to a quartz cylindrical cell with a path length of 1 mm. The CD spectra of CADP-10 and CADP-7 were detected by the spectrometer V100 instrument (Rudolph Autopol IV-T).

Cryo-Electron Microscope (Cryo-EM) Images of CADP-10 and CADP-7. CADP-10 and CADP-7 were dissolved in PBS buffer (pH = 7.4) at a final concentration of 128 μM. Then, 5 μL of the peptide solutions were transferred to the electron microscopy grids, and then these grids were placed into a cryo-holder. Finally, the morphology of peptides was observed by a 200 kV Cryo-EM (CRYO-EM001, ThermoFisher).

Bacteria Strains. Methicillin-resistant *Staphylococcus aureus* USA 300 (MRSA), *Escherichia coli* ATCC 25922, methicillin-resistant *Staphylococcus aureus* ATCC 43300, *Enterococcus faecalis* ATCC 29212, *Pseudomonas aeruginosa* ATCC 27835, and *Klebsiella pneumoniae* ATCC 13883 were bought from Hangzhou Biosci Biotechnology Co., Ltd. Multidrug-resistant *Escherichia coli* BNCC 186732 (MRE), *Enterobacter cancerogenus* ATCC 35317, *Salmonella typhimurium* BNCC 1344, and *Staphylococcus epidermidis* ATCC 12228 were purchased from Beijing Beina Chuanglian Biotechnology Institute.

Minimum Inhibitory Concentration (MIC) and Minimum Bactericidal Concentration (MBC) Determination. The MIC and MBC of peptides against bacteria were determined by a standard microdilution method provided by the Clinical and Laboratory Standards Institute.[39,40] Briefly, peptides were prepared at different concentrations (2 μM, 4 μM, 8 μM, 16 μM, 32 μM, 64 μM, 128 μM, 256 μM, 512 μM, and 1024 μM) in PBS buffer. Next, 100 μL of the solution at different concentrations was added to a 96-well plate. 100 μL of the mid logarithmic growth-phase culture of bacteria at 1×10^6 CFU mL^{-1} in BHI broth were added into the 96-well plate. The plate was incubated in an incubator at 37 °C for 18 h. The concentration in the lowest concentration group of the peptides with no visible growth was referred to as the MIC of the peptide against the bacteria. In addition, 10 μL of suspension from each group was spread on the solid BHI agar plates. These plates were incubated in an incubator at 37 °C for 24 h. The concentration in the lowest concentration group of peptides without bacterial colony growth was referred to as the MBC of the peptide against the bacteria. The experiment was repeated three times to give the MICs and MBCs.

Bacterial Growth Curves under the Treatment of Peptides. First, CADP-7 and CADP-10 were prepared at 640 μM in PBS buffer, and 20 μL of peptide solutions was added into a 96-well plate. Next, the mid logarithmic growth-phase MRSA and MRE were prepared at 1×10^6 CFU mL^{-1} in Luria−Bertani (LB) broth, respectively. 180 μL of these bacterial suspensions was added to the 96-well plate. The plate was incubated in an incubator at 37 °C for 24 h. Every 2 h, the optical density at 600 nm (OD_{600}) of the plate was recorded by a microplate reader (Varioskan Lux, ThermoFisher). Meanwhile, at 8 h, 5 μL diluted bacterial suspension from the Control group, CADP-7 group, and CADP-10 group were spread on solid LB agar plates. These plates were incubated in an incubator at 37 °C for 24 h. The number of colony-forming units (CFU) was quantified for evaluating bacterial viability. The minimum detection of bacterial concentration was 100 CFU mL^{-1}.

Bactericidal Activity of CADP-7 and CADP-10 against Persisters. The mid logarithmic growth-phase MRSA and MRE were prepared at 1×10^6 CFU mL^{-1} in Luria−Bertani (LB) broth, respectively. 200 μL of these bacterial suspension was added to the 96-well plate. The plate was incubated in an incubator at 37 °C for 72 h. Every 24 h, the medium in the plate was removed, then washed 3 times with PBS, and a new medium was added. After the incubation, the medium in the plate was removed, then washed 3 times with PBS, and 200 μL of LB broth containing 100 × MICs of rifampicin was added.[41] After 24 h of coculturation, the rifampicin solution was removed, and the bacteria adherent to the plate were dislodged. The surviving bacteria were collected as the persisters. Peptide solutions were added into the bacterial suspension at a concentration of 128 μM and coincubated for 2 h. After coincubation, 5 μL diluted bacterial suspension from the Control group, CADP-7 group, and CADP-10 group were spread on solid LB agar plates. These plates were incubated in an incubator at 37 °C for 24 h. The number of colony-forming units (CFU) was quantified for evaluating bacterial viability. The minimum detection of bacterial concentration was 100 CFU mL^{-1}. The experiment was independently repeated three times.

Antibiofilm Activity of CADP-7 and CADP-10. The mid logarithmic growth-phase MRSA and MRE were prepared at 1×10^6 CFU mL^{-1} in Luria−Bertani (LB) broth, respectively. One mL of the bacterial suspension was added to confocal dishes (35 mm). The dishes were incubated in an incubator at 37 °C for 72 h. Every 24 h, the medium in the dishes was removed, then washed 3 times with PBS, and a new medium was added. After the incubation, the medium in the dishes was removed, then washed 3 times with PBS. One mL of PBS containing CADP-7 (128 μM) or CADP-10 (128 μM) was added to the dishes and coincubated for 2 h, respectively. After coincubation, the bacteria adherent to the plate were dislodged. Five μL diluted bacterial suspension from the Control group, CADP-7 group, and CADP-10 group were spread on solid LB agar plates. These plates were incubated in an incubator at 37 °C for 24 h. The number of colony-forming units (CFU) was quantified for evaluating bacterial viability. The minimum detection of bacterial concentration was 100 CFU mL^{-1}.

The mid logarithmic growth-phase MRSA and MRE were prepared at 1×10^6 CFU mL^{-1} in Luria−Bertani (LB) broth, respectively. One mL of the bacterial suspension was added to confocal dishes (35 mm). The dishes were incubated in an incubator at 37 °C for 72 h. Every 24 h, the medium in the dishes was removed, then washed 3 times with PBS, and a new medium was added. After the incubation, the medium in the dishes was removed, then washed 3 times with PBS. One mL of PBS containing CADP-7 (128 μM) or CADP-10 (128 μM) was added to the dishes and coincubated for 2 h, respectively. After coincubation, the treated biofilms were washed 3 times with PBS and stained with a LIVE/DEAD BacLight bacterial viability kit (Invitrogen). Next, the biofilms were observed using a confocal laser scanning microscope (Zeiss LSM 800).

Crystal Violet Staining of Biofilms. The mid logarithmic growth-phase MRSA and MRE were prepared at 1×10^6 CFU mL^{-1} in Luria−Bertani (LB) broth, respectively. 200 μL of these bacterial suspension was added to 96-well plates. The plates were incubated in an incubator at 37 °C for 72 h. Every 24 h, the medium in the plate was removed, then washed 3 times with PBS, and a new medium was added. After the incubation, the medium in the plate was removed, then washed 3 times with PBS. One mL of PBS containing CADP-7 (128 μM) or CADP-10 (128 μM) was added to the plates and coincubated for 2 h, respectively. After coincubation, 100 μL of 10% crystal violet bacterial suspension in the plates was removed and the 96-well plates were washed with PBS three times. Next, 100 μL of 95% ethyl alcohol (deionized water) were added to the plates to

https://doi.org/10.1021/acsnano.4c18858
ACS Nano XXXX, XXX, XXX−XXX

dissolve the crystal violet. Finally, the optical density at 595 nm (OD_{595}) of each well in the plates was recorded using a microplate reader (Varioskan Lux, ThermoFisher). The experiment was independently repeated three times.

Rapid Antibacterial Experiment of CADP-10 *In Vitro*. The mid logarithmic growth-phase MRSA was prepared at 5×10^8 CFU mL^{-1} in PBS. Then, 900 μL of MRSA suspension was added to sterile glass bottles. The mid logarithmic growth-phase MRE was prepared at 1×10^8 CFU mL^{-1} in PBS. Then, 900 μL of MRE suspension was added to sterile glass bottles. 100 μL of CADP-10 (1280 μM) and CADP-7 (1280 μM) were added to the glass bottles, respectively. The glass bottles were placed in an incubator for 2 h. At 0, 15, 30, 60, and 120 min, 5 μL diluted bacterial suspension from the Control group, CADP-7 group, and CADP-10 group were spread on solid LB agar plates. These plates were incubated in an incubator at 37 °C for 24 h. The number of colony-forming units (CFU) was quantified for evaluating bacterial viability. The minimum detection of bacterial concentration was 100 CFU mL^{-1}. The experiment was independently repeated three times.

Morphology of Bacteria Treated with Peptides. The mid logarithmic growth-phase MRSA was prepared at 5×10^8 CFU mL^{-1} in PBS. Then, 900 μL of MRSA suspension was added to sterile glass bottles. The mid logarithmic growth-phase MRE was prepared at 1×10^8 CFU mL^{-1} in PBS. Then, 900 μL of MRE suspension was added to sterile glass bottles. 100 μL of CADP-10 (1280 μM) and CADP-7 (1280 μM) were added to the glass bottles, respectively. The glass bottles were placed in an incubator for 2 h. The peptide solution was removed, and PBS was used to wash the bottle three times. Next, 2.5% glutaraldehyde was used to fix the bacteria for 2 h, and ethanol solutions at different concentrations (10%, 30%, 50%, 70%, 90%, and 100%) dehydrated the bacteria, respectively. Finally, the bacterial suspension was dripped onto the silicon wafer, and a field emission scanning electron microscope (FE-SEM, GeminiSEM 450) was used to observe the morphology of the treated bacteria.

Intracellular ATP Level Measurement. The mid logarithmic growth-phase MRSA was prepared at 5×10^8 CFU mL^{-1} in PBS. Then, 450 μL of MRSA suspension was added to 1.5 mL EP tubes. The mid logarithmic growth-phase MRE was prepared at 1×10^8 CFU mL^{-1} in PBS. Then, 450 μL of MRE suspension was added to 1.5 mL EP tubes. 50 μL of CADP-10 (1280 μM) and CADP-7 (1280 μM) were added to the tubes, respectively. The tubes were placed in an incubator for 2 h. The tubes were centrifuged at 7000 r.mp (5 min). The supernatant was removed, and PBS was used to wash the tubes three times. Following the manufacturer's approach provided by the ATP Assay Kit (Beyotime, catalog no. S0026), the ATP levels in the treated bacteria were measured.

Zeta Potential of Bacteria Treated with CADP-10. The mid logarithmic growth-phase MRSA was prepared at 5×10^8 CFU mL^{-1} in PBS. Then, 450 μL of MRSA suspension was added to 1.5 mL EP tubes. The mid logarithmic growth-phase MRE was prepared at 1×10^8 CFU mL^{-1} in PBS. Then, 450 μL of MRE suspension was added to 1.5 mL EP tubes. 50 μL of CADP-10 (1280 μM) and CADP-7 (1280 μM) were added to the tubes, respectively. The tubes were placed in an incubator for 2 h. 50 μL of CADP-10 (1280 μM) and CADP-7 (1280 μM) were added to the tubes containing 450 μL of PBS. The Zeta potential of the suspension in these tubes was measured using a Zeta Nanosizer (LHA19110041, Brookhaven).

Changes in the Membrane Permeability of Treated Bacteria. The mid logarithmic growth-phase MRSA and MRE were prepared at 1×10^8 CFU mL^{-1} in 5 mM HEPES buffer (pH = 7.4) containing 5 mM glucose, respectively. 900 μL of bacterial suspension was added to 1.5 mL EP tubes. Next, 10 μL of 1-(*N*-phenylamino) naphthalene (NPN) solution was added to the tubes and coincubated for 30 min. 100 μL of CADP-10 solution (1280 μM) and CADP-7 solution (1280 μM) were added to the tubes, respectively. After 2 h of coculture, the Spectrofluorometer (Edinburgh, F55) was used to the fluorescent intensity of NPN (λex = 350 nm, λem = 420 nm) in the Control group, CADP-7 group and CADP-10 group, respectively.

Changes in the Membrane Potential of Treated Bacteria. The mid logarithmic growth-phase MRSA and MRE were prepared at 1×10^8 CFU mL^{-1} in 5 mM HEPES buffer (pH = 7.4) containing 20 mM glucose and 0.1 mM KCl, respectively. 900 μL of bacterial suspension was added to 1.5 mL EP tubes. Ten μL of the membrane-potential-sensitive dye DiSC3(5) solution (2 μM) was added to the tubes, followed by 30 min of coculture for integrating DiSC3(5) into bacterial membranes. Finally, 100 μL of CADP-10 solution (1280 μM) and CADP-7 solution (1280 μM) were added to the tubes, respectively. The fluorescent intensity (λex = 622 nm, λem = 670 nm) of the mixture suspension in these tubes was measured using a Spectrofluorometer (Edinburgh, F55).

Intracellular ROS Measurement. The mid logarithmic growth-phase MRSA and MRE were prepared at 2×10^8 CFU mL^{-1} in PBS buffer, respectively. 500 μL of bacterial suspension was added into 1.5 mL EP tubes containing 10 μL of DCFH-DA solution (10 mM), followed by 30 min of coculture. Then, the EP tubes were centrifuged to remove the solution containing DCFH-DA. 500 μL of CADP-10 solution (128 μM) and CADP-7 solution (128 μM) were added to the tubes and cocultured for 2 h. Finally, Following the manufacturer's approach provided by a ROS Assay Kit (Beyotime, S0033S), the fluorescence intensity (λex = 488 nm, λem = 530 nm) of the tubes was measured using a microplate reader (Varioskan Lux, ThermoFisher).

Transmission Electron Microscopy (TEM). The mid logarithmic growth-phase MRSA was prepared at 5×10^8 CFU mL^{-1} in PBS. Then, 450 μL of MRSA suspension was added to 1.5 mL EP tubes. The mid logarithmic growth-phase MRE was prepared at 1×10^8 CFU mL^{-1} in PBS. Then, 450 μL of MRE suspension was added to 1.5 mL EP tubes. 50 μL of CADP-10 (1280 μM) and CADP-7 (1280 μM) were added to the tubes, respectively. The tubes were placed in an incubator for 2 h. The tubes were centrifuged at 7000 r.mp (5 min). The supernatant was removed, and PBS was used to wash the tubes three times. Finally, 500 μL of 2.5% glutaraldehyde solution was added to the tubes of all groups and coincubated for 12 h. After the coincubation, the tubes were centrifuged at 7000 r.mp (5 min), the supernatant was removed, and 1% osmic acid was added to the tubes. Ethanol solutions at different concentrations (10%, 30%, 50%, 70%, 90%, and 100%) dehydrated the bacteria, respectively. Finally, the bacteria were cut into pieces (~ 60 nm), placed on the ultrathin sliced copper grids. The bacterial morphology was observed by a transmission electron microscope.[42]

Cytotoxicity of CADP-10 Test. Human bone mesenchymal stem cells (hBMSC) were provided by the Yang's research group at the Union Hospital, Tongji Medical School, Huazhong University of Science and Technology. According to the previous reference,[43−45] the bone marrow-derived macrophages (BMDMs) in mice (about 6 weeks, BALB/c) were extracted and cultured in DMEM containing 10% FBS and M-CSF (10 ng mL^{-1}). hBMSC and BMDMs were seeded in 96-well plates (10,000 cells $well^{-1}$) and incubated for 24 h. Then, the medium in the plates was removed, and 100 μL of fresh medium containing peptides at different concentrations (2 μM, 4 μM, 8 μM, 16 μM, 32 μM, 64 μM, 128 μM, 256 μM, 512 μM, and 1024 μM) was added to the plates. The plates were placed in an incubator and incubated for 24 h. Ten microliters of thiazolyl blue tetrazolium bromide solution (5 mg mL^{-1} in PBS) was added to the plates and incubated for 4 h. Finally, 100 μL of SDS-HCl solution (10% SDS and 0.01 M HCl) was added to the plates for dissolving formazan in each well of the plates. The plates were placed in an incubator for 24 h. The optical density at 595 nm (OD_{595}) of each well in the plates was recorded using a microplate reader (Varioskan Lux, ThermoFisher). The experiment was independently repeated three times.

Hemolytic Activity of CADP-10 Test. The fresh New Zealand rabbit whole blood was washed with 0.9% saline and resuspended to PBS. The fresh New Zealand rabbit whole blood was prepared at 4% using PBS. 500 μL of 4% blood suspension was combined with 500 μL of CADP-7 (640 μM) in the 1.5 mL EP tube and CADP-10 (640 μM) in the 1.5 mL EP tube, respectively. 500 μL of 4% blood suspension combined with 500 μL of 1% tritonX-100 in the 1.5 mL EP tube was as the positive control. 500 μL of 4% blood suspension

https://doi.org/10.1021/acsnano.4c18858
ACS Nano XXXX, XXX, XXX−XXX

combined with 500 μL of PBS in the 1.5 mL EP tube was as the negative control. Next, these tubes were placed in an incubator at 37 °C for 3 h. After incubation, these tubes were centrifuged at 10000 r.p.m. for 10 min. The absorbance at 570 nm of the suspension from the tubes was measured by a microplate reader (Varioskan Lux, ThermoFisher). The experiment was independently repeated three times to calculate the hemolytic rate of CADP-10 and CADP-7 based on the formula[46]

$$\text{hemolysis rate } (\%) = \frac{OD_a - OD_1}{OD_0 - OD_1} \times 100\%$$

The OD_a is the optical density (OD) at 570 nm of the tested samples, the OD_1 was the optical density (OD) at 570 nm of the negative control, and the OD_0 was the optical density (OD) at 570 nm of the positive control.

mRNA Expression of Polarized Macrophage. The bone marrow-derived macrophages (BMDMs) in mice (about 6 weeks, BALB/c) were extracted and cultured in DMEM containing 10% FBS and M-CSF (10 ng mL^{-1}). BMDMs were seeded in 6-well plates (200,000 cells $well^{-1}$) and incubated for 24 h. Next, we added CADP-10 (128 μM) to the wells in the plates and coincubated for 24 h. The wells with the addition of LPS (final concentration: 100 ng mL^{-1}) were positive controls for M1-type polarization stimulation. The wells with the addition of IL-4 (final concentration: 20 ng mL^{-1}) were positive controls for M2-type polarization stimulation. Following the manufacturer's approach, the total mRNA in BMDMs from each group was extracted using TRIzol reagent (Invitrogen, Carlsbad, CA). The PrimeScript RT Reagent Kit (Takara) was used to reverse-transcribe mRNA (Table S1), and cDNA was synthesized. The SYBR Premix Ex Taq (TAKARA) performed the qPCR using a StepOnePlus Real-Time PCR system (Applied Biosystems). We used the expression level of β-Actin to normalize the relative expression of mRNA. The experiment was independently repeated three times.

Osteogenic Differentiation of hBMSC *In Vitro*. hBMSC were seeded in 48-well plates and cultured for 24 h. Next, the old medium was removed, and the osteogenic differentiation medium containing CADP-10 at different concentrations (8 μM, 16 μM, and 32 μM) was added to the wells in the plates, respectively. The plates were placed in a cell incubator for 7 days. Then, the old medium was removed, and the cells were washed with PBS three times, followed by fixing them in 4% paraformaldehyde for 30 min. Finally, following the manufacturer's approach provided by an ALP staining kit (Beyotime), the ALP in cells was stained. An optical microscope was used to observe the cells. For the ALP activity measurement, IP cell lysate without protein inhibitors was used to lyse adherent cells. The plates were centrifuged. Ten μL of cell supernatant from each well in plates was mixed with buffer solution in 96-well plates and coincubated for 15 min. Finally, a color-developing agent was added to each well in the 96-well plates, and the optical density at 520 nm (OD_{520}) of each well in the plates was recorded using a microplate reader (Varioskan Lux, ThermoFisher).

hBMSCs were seeded in 48-well plates and cultured for 24 h. Next, the old medium was removed, and the osteogenic differentiation medium containing CADP-10 at different concentrations (8 μM, 16 μM, and 32 μM) was added to the wells in the plates, respectively. The plates were placed in a cell incubator for 21 days. Then, the old medium was removed and the cells were washed with PBS three times, followed by fixing them with 4% paraformaldehyde for 30 min. Finally, adherent cells were stained with 0.2% alizarin red S solution (Solarbio) for 30 min, which was observed by an optical microscope. The water was drained from the plates, and 10% cetylpyridinium chloride (CPC) solution was added. The plates were placed on a shaker and gently shaken for 30 min. The optical density at 562 nm (OD_{562}) of each well in the plates was recorded using a microplate reader (Varioskan Lux, ThermoFisher).

Immunofluorescence Staining of hBMSC Treated with CADP-10. hBMSC were seeded in 6-well plates (50,000 cells $well^{-1}$) and incubated for 24 h. Then, the old medium was removed, and the osteogenic differentiation medium containing CADP-10 at different concentrations (8 μM, 16 μM, and 32 μM) was added to the wells in the plates, respectively. The plates were placed in a cell incubator for 14 days. Then, the old medium was removed and the cells were washed with PBS three times, followed by fixing them with 4% paraformaldehyde for 30 min. The adherent cells were permeated using 0.5% tritonX-100 and sealed for 20 min. RUNX2 antibody was added to each well in the plates and coincubated at 4 °C for 12 h. 100 μL of anti-rabbit antibody with green fluorophore group was added to each well and incubated at 25 °C for 1 h, followed by washing with 0.1% PBST. The adherent cells were stained with DAPI (Solarbio) and phalloidin (Solarbio). Next, the cells were observed using a laser scanning confocal microscope (Zeiss LSM 800).

Osteogenesis and Biosafety of CADP-10 *In Vivo*. The animal experiments were conducted under the guidance of the Institutional Animal Care and Use Committee (IACUC) and Laboratory Animal Ethics at Zhejiang Academy of Traditional Chinese Medicine. The acceptance number is 2023−170(K)-X1. The male, 6−8 weeks old, New Zealand white rabbits with a weight of 1.8−2.3 kg were provided by Zhejiang Chinese Medical University Laboratory Animal Research Center. Nine male New Zealand white rabbits were randomly divided into three groups (3 rabbits per group): the Healthy group without any operation, the Control group (sham operation), and the CADP-10 group. First, the rabbits in the three groups were anesthetized by inhaling isoflurane. After the rabbit was anesthetized entirely, the hair on the hind legs of the rabbit was shaved with a razor and disinfected with iodophor. Then, we found the tibial platform on the rabbit's leg bone and drilled a small hole with a diameter of 2 mm into the tibial platform with a medical drill on day 0. These holes in the rabbit's tibia were sealed with bone wax. Through this hole, 100 μL of CADP-10 (128 μM) was delivered by injection into the bone marrow cavity of rabbits in the CADP-10 group to promote the healing of rabbit leg bones on day 2. 100 μL of 0.9% saline was delivered by injection into the bone marrow cavity of rabbits in the Control group. On day 2, day 4, and day 10, the whole blood from rabbits in each group was collected for the blood routine test, respectively. On day 10, the rabbit's tibias from each group were scanned by a Bruker Micro-CT SkyScan 1176 imaging system. SkyScan CT Analyzer software analyzed the data about tibias and reconstructed 3D images. Moreover, these tibia samples were decalcified with EDTA for one month. Then, these samples were embedded, sliced, stained with H&E, and finally viewed using an optical microscope.

Mouse Macrophage Flow Cytometry Experiment. According to the previous reference, the bone marrow-derived macrophages (BMDMs) in mice (about 6 weeks, BALB/c) were extracted and cultured in DMEM containing 10% FBS and M-CSF (10 ng mL^{-1}). First, BMDMs were seeded in 6-well plates (20,000 cells $well^{-1}$) and incubated for 24 h. For the Control group, the old medium was removed, and the fresh medium was added to the wells in the plates. For the positive control of M1 macrophage (the LPS group), the fresh medium containing LPS (100 ng mL^{-1}) was added to the wells in the corresponding plates. For the positive control of M2 macrophage (the IL-4 group), the fresh medium containing IL-4 (20 ng mL^{-1}) was added to the wells in the corresponding plates. For the MRSA group, the fresh medium containing MRSA (1×10^6 CFU mL^{-1}) was added to the wells in the corresponding plates. For the CADP-10@MRSA group, CADP-10 (128 μM) and MRSA (1×10^6 CFU mL^{-1}) were added to the medium and coincubated for 30 min, and the medium was added to the wells in the corresponding plates. Moreover, for the MRE group, the fresh medium containing MRE (1×10^6 CFU mL^{-1}) was added to the wells in the corresponding plates. For the CADP-10@MRE group, CADP-10 (128 μM) and MRE (1×10^6 CFU mL^{-1}) were added to the medium and coincubated for 30 min, and the medium was added to the wells in the corresponding plates. These plates were placed in an incubator at 37 °C for 24 h. Especially for the MRSA/CADP-10 group, the fresh medium containing MRSA (1×10^6 CFU mL^{-1}) was added to the wells in the corresponding plates and coincubated for 12 h. Next, the CADP-10 (final concentration: 128 μM) was added to these plates, mixed, and coincubated for another 12 h. For the MRE/CADP-10 group, the fresh medium

https://doi.org/10.1021/acsnano.4c18858
ACS Nano XXXX, XXX, XXX−XXX

containing MRE (1×10^6 CFU mL^{-1}) was added to the wells in the corresponding plates and coincubated for 12 h. Next, the CADP-10 (final concentration: 128 μM) was added to these plates, mixed, and coincubated for another 12 h. The adherent BMDMs were dislodged and stained with anti-CD16/CD32 (BD Pharmingen), anti-CD86-PE (BD Pharmingen), anti-CD-80-FITC (BD Pharmingen), anti-CD206-APC (BD Pharmingen), and anti-iNOS-Cy7 (BD Pharmingen). The collected BMDMs were analyzed using a flow cytometry analyzer (CytoFLEX LX, Beckman Coulter). The supernatant from each well in plates of all groups was collected for anti-inflammatory and pro-inflammatory analysis. Enzyme-linked immunosorbent assays (TNF-α, IL-6, and IL-12) were employed to measure cytokine secreted by BMDMs in the supernatant.

Dissociation Constant between CADP-10 and Bacterial Antigen Determination. We used a MicroCal PEAQ-ITC (Malvern) instrument to conduct the isothermal titration calorimetry (ITC) experiments to determine dissociation constant between CADP-10 and bacterial antigen. CADP-10 was prepared into HEPES solution (10 mM) at the concentration of 50 μg mL^{-1}. The solution was added to the cell of the MicroCal PEAQ-ITC and the temperature of the cell was set to 25 °C. Next, LPS was prepared into HEPES solution (10 mM) at the concentration of 500 μg mL^{-1}, and then, the solution was added into the syringe of the MicroCal PEAQ-ITC. The substrate was continuously injected in 19 injections of 3 μL. The MicoCal PEAQ-ITC Analysis Software was used to process these heat data and then gave the dissociation constant for CADP-10 and LPS.[47,48] CADP-10 was prepared into HEPES solution (10 mM) at the concentration of 50 μg mL^{-1}. The solution was added to the cell of the MicroCal PEAQ-ITC and the temperature of the cell was set to 25 °C. Next, LTA was prepared into HEPES solution (10 mM) at the concentration of 250 μg mL^{-1}, and then, the solution was added into the syringe of the MicroCal PEAQ-ITC. The substrate was continuously injected in 19 injections of 3 μL. The MicoCal PEAQ-ITC Analysis Software was used to process these heat data and then gave the dissociation constant for CADP-10 and LTA.

PCR Array Plate Experiment. The bone marrow-derived macrophages (BMDMs) in mice (about 6 weeks, BALB/c) were extracted and cultured in DMEM containing 10% FBS and M-CSF (10 ng mL^{-1}). First, BMDMs were seeded in 6-well plates (20,000 cells well^{-1}) and incubated for 24 h. For the LTA group, the old medium was removed, and the fresh medium containing 100 ng mL^{-1} of LTA was added to the wells in the plates. For the LTA + CADP-10 group, the old medium was removed, and the fresh medium containing 100 ng mL^{-1} of LTA and 128 μM of CADP-10 was added to the wells in the plates. For the LPS group, the old medium was removed, and the fresh medium containing 100 ng mL^{-1} of LPS was added to the wells in the plates. For the LPS + CADP-10 group, the old medium was removed, and the fresh medium containing 100 ng mL^{-1} of LPS and 128 μM of CADP-10 was added to the wells in the plates. These plates were placed in an incubator at 37 °C for 24 h. Following the manufacturer's approach, the total mRNA in BMDMs from each group was extracted using TRIzol reagent (Invitrogen, Carlsbad, CA). The PrimeScript RT Reagent Kit (Takara) was used to reverse-transcribe mRNA, and cDNA was synthesized. PCR array (WC-MRNA0148-M, WCGENE Biotech) was used to determine the mRNA expression according to the manufacturer's approach.

Interaction between Mag-CADP-10 and Bacteria. First, CADP-10 was covalently attached to magnetic beads (200 nm) to form Mag-CADP-10 based on the method provided by the manufacturer (Beyotime Biotechnology). Bacteria was prepared in PBS at the concentration of 1×10^8 CFU mL^{-1}. Next, the bacteria suspension was added to the glass bottles. Mag and Mag-CADP-10 were added to the glass bottles, respectively. The glass bottles were placed in the oscillator for 1 min to mix the bacteria with magnetic beads. We put magnets on the bottom of these glass bottles and recorded the changes in the glass bottles. The optical density at 600 nm (OD_{600}) of the suspension from the bottles was recorded using a microplate reader (Varioskan Lux, ThermoFisher). The experiment was independently repeated three times. Finally, the bacterial suspension from all groups was dripped onto the silicon wafer. The field emission scanning electron microscope (FE-SEM, GeminiSEM 450) was used to observe the morphology of the treated bacteria.

Antibacterial Activity of CADP-10 in Rabbit Bone Marrow Cavity *In Vitro*. The male, 6−8 weeks old, New Zealand white rabbits with a weight of 1.8−2.3 kg were provided by Zhejiang Chinese Medical University Laboratory Animal Research Center. First, the rabbits in the three groups were anesthetized by inhaling isoflurane. After the rabbit was anesthetized entirely, the hair on the hind leg of the rabbit was shaved with a razor and disinfected with iodophor. Then, we found the tibial platform on the rabbit's leg bone and drilled a small hole with a diameter of 5 mm into the tibial platform with a medical drill. Through this small hole, we extracted the bone marrow fluid from the bone marrow cavity of the tibia and mixed it into 1 mL of PBS, then stirred it evenly. The mid logarithmic growth-phase MRSA was added to the PBS buffer (final concentration: ~1×10^8 CFU mL^{-1}). Finally, CADP-7 (final concentration: 128 μM), CADP-10 (final concentration: 128 μM), and CADP-10 (final concentration: 256 μM) were added to the corresponding tubes containing the PBS buffer, respectively. The tubes were placed in an incubator and cultured for 4 h. At 0, 1, and 4 h, 5 μL diluted bacterial suspension from the Control group, the CADP-7 (128 μM) group, the CADP-10 (128 μM) group, and the CADP-10 (256 μM) group were spread on solid LB agar plates. These plates were incubated in an incubator at 37 °C for 24 h. The number of colony-forming units (CFU) was quantified for evaluating bacterial viability. The minimum detection of bacterial concentration was 100 CFU mL^{-1}.

Bacterial Acquired Drug Resistance Experiment. First, we selected a commercially available antibiotic, gentamicin (Gen), as a positive control. According to the MIC test method described above, we first measured the MIC of Gen and CADP-10 against MRSA.[49] The sub-MIC (1/2 MIC) of Gen and CADP-10 was determined. Then, the mid logarithmic growth-phase MRSA from the sub-MIC (1/2 MIC) group was used to test the new MIC of Gen and CADP-10 according to the MIC test method described above. The new MIC and new sub-MIC of Gen and CADP-10 were determined. Then, the mid logarithmic growth-phase MRSA from the new sub-MIC (1/2 MIC) group was used to test another MIC of Gen and CADP-10 according to the MIC test method described above. We got the MIC and sub-MIC of Gen and CADP-10 again. We call getting a MIC value one time and repeat it like this 30 times.

Models of Osteomyelitis Infection in Rabbits. The animal experiments were conducted under the guidance of the Institutional Animal Care and Use Committee (IACUC) and Laboratory Animal Ethics at Zhejiang Academy of Traditional Chinese Medicine. The acceptance number is 2023−170(K)-X1. The male, 6−8 weeks old, New Zealand white rabbits with a weight of 1.8−2.3 kg were provided by Zhejiang Chinese Medical University Laboratory Animal Research Center. Nine male New Zealand white rabbits were randomly divided into three groups (20 rabbits per group): the Control group (sham operation), the CADP-7 group, the Van group, and the CADP-10 group. First, the rabbits in the three groups were anesthetized by inhaling isoflurane. After the rabbit was anesthetized entirely, the hair on the hind legs of the rabbits was shaved with a razor and disinfected with iodophor. Then, we found the tibial platform on the rabbit's leg bone and drilled a small hole with a diameter of 2 mm into the tibial platform with a medical drill. Through the hole, 50 μL of MRSA suspension was delivered into the marrow cavity of rabbits to cause osteomyelitis, and the osteomyelitis was established on day 0. These holes in the rabbit's tibia were sealed with bone wax.

We treated these rabbits with osteomyelitis on day 1. For the Control group, 100 μL of 0.9% saline was delivered to the marrow cavity through the holes. For the CADP-7 group, 100 μL of CADP-7 (128 μM) was delivered to the marrow cavity through the holes. For the CADP-10 group, 100 μL of CADP-10 (128 μM) was delivered to the marrow cavity through the holes. For the Van group, 100 μL of Van (10 mg mL^{-1}) was delivered to the marrow cavity through the holes. On day 2, some rabbits in each group (n = 5) were euthanized after treatment, and the tissue in the tibial cavity was extracted with 1 mL of PBS. The tissue in PBS was then homogenized. Five μL diluted

https://doi.org/10.1021/acsnano.4c18858
ACS Nano XXXX, XXX, XXX−XXX

bacterial suspension from the Control group, the CADP-7 group, the Van group, and the CADP-10 group were spread on solid LB agar plates, respectively. These plates were incubated in an incubator at 37 °C for 24 h. The number of colony-forming units (CFU) was quantified for evaluating bacterial viability. The minimum detection of bacterial concentration was 100 CFU mL^{-1}.

Next, on day 2, day 7, and day 14, the whole blood from rabbits in each group was collected for the blood routine test, respectively. Enzyme-linked immunosorbent assays (TNF-α, IL-6, CRP, and IL-1β) were employed to measure cytokine in serum. On day 14, the rabbits tibias from each group were scanned by a Bruker Micro-CT SkyScan 1176 imaging system. SkyScan CT Analyzer software analyzed the data about tibias and reconstructed 3D images. Moreover, the rabbit tibias from each group were scanned by magnetic resonance imaging (MRI, WANDONG, i_Space 1.5T). Finally, these tibia samples were decalcified with EDTA for one month, and then these samples were embedded, sliced, stained with H&E, and finally viewed using an optical microscope.

ASSOCIATED CONTENT

Supporting Information

The Supporting Information is available free of charge at https://pubs.acs.org/doi/10.1021/acsnano.4c18858.

Movies of different Mag interacted with MRSA (Video S1) (MP4)

Movies of different Mag interacted with MRSA (Video S2) (MP4)

Movies of different Mag interacted with MRSA (Video S3) (MP4)

Movies of different Mag interacted with MRSA (Video S4) (MP4)

Design of primers in PCR experiments (Table S1); characterization of peptides (Figure S1); the antibacterial activity of CADP-7 and CADP-10, and crystal violet staining of the bacterial biofilm treated with CADP-7 and CADP-10 (Figure S2); the zeta potential of bacteria treated with CADP-10 and the rapid antibacterial activity of CADP-7 and CADP-10 (Figure S3); ROS measurement in bacteria treated with CADP-7 and CADP-10 (Figure S4); mRNA levels in the bone marrow-derived macrophages (BMDMs) under the treatment of CADP-7 and CADP-10 (Figure S5); the percentage of RUNX-2^+ in the nucleus of the cells measurement and the trabecular separation analysis (Figure S6); The platelet (PLT) count and white blood cell (WBC) count in the rabbit whole blood (Figure S7); the flow cytometry analysis of $CD86^+$ macrophages and $CD80^+$ macrophages in the total macrophages (Figure S8); the concentration of IL-6 secreted by BMDMs and the OD_{600} of the bacterial suspension (Figure S9); the viability of bacteria in bone marrow tissue fluid measurement and the bacterial resistance acquisition measurement (Figure S10); the RBC count, the PLT count, and the concentration of HGB in whole blood of rabbits (Figure S11) (PDF)

AUTHOR INFORMATION

Corresponding Author

Huaimin Wang − *Department of Chemistry, School of Science, Institute of Natural Sciences, Westlake Institute for Advanced Study, Westlake University, Hangzhou 310024 Zhejiang Province, China;* orcid.org/0000-0002-8796-0367; Email: wanghuaimin@westlake.edu.cn

Authors

Ziao Zhou − *Department of Chemistry, Zhejiang University, Hangzhou 310027 Zhejiang Province, China; Department of Chemistry, School of Science, Institute of Natural Sciences, Westlake Institute for Advanced Study, Westlake University, Hangzhou 310024 Zhejiang Province, China*

Peng Zhang − *Department of Chemistry, School of Science, Institute of Natural Sciences, Westlake Institute for Advanced Study, Westlake University, Hangzhou 310024 Zhejiang Province, China*

Dinghao Chen − *Department of Chemistry, School of Science, Institute of Natural Sciences, Westlake Institute for Advanced Study, Westlake University, Hangzhou 310024 Zhejiang Province, China*

Nan Kong − *Department of Chemistry, School of Science, Institute of Natural Sciences, Westlake Institute for Advanced Study, Westlake University, Hangzhou 310024 Zhejiang Province, China*

Huayang Liu − *Department of Chemistry, School of Science, Institute of Natural Sciences, Westlake Institute for Advanced Study, Westlake University, Hangzhou 310024 Zhejiang Province, China*

Juan Liang − *Department of Chemistry, School of Science, Institute of Natural Sciences, Westlake Institute for Advanced Study, Westlake University, Hangzhou 310024 Zhejiang Province, China*

Kai Huang − *Department of Orthopedics, Tongde Hospital of Zhejiang Province, Hangzhou 310012, China*

Complete contact information is available at: https://pubs.acs.org/10.1021/acsnano.4c18858

Author Contributions

‖Z.Z. and P.Z. contributed equally. H.W. conceived the project. Z.Z. designed and conducted the related experiments. Z.Z. and D.C. synthesized and characterized the peptides. Z.Z. and H.L. conducted all the bacterial experiments. D.C., N.K., J.L., and Z.Z. performed some cell experiments. Z.Z. and P.Z. performed the animal experiments. H.W. and Z.Z. analyzed the date and wrote the manuscript with input from the other authors. All the authors discussed the results and had agreement on the final version of the manuscript.

Notes

The authors declare the following competing financial interest(s): Z.A. Zhou and H.M.Wang appled a patent based on this work.

ACKNOWLEDGMENTS

This project was supported by Zhejiang Provincial Natural Science Foundation of China under Grant No XHD23C1001 and the National Natural Science Foundation of China (82272145), Westlake Education Foundation. We thank the Instrumentation and Service Center for Molecular Sciences, Instrumentation and Service Center for Physical Sciences, and Biomedical Research Core Facilities at Westlake University for the assistance with measurements.

REFERENCES

(1) Masters, E. A.; Ricciardi, B. F.; Bentley, K. L. d. M.; Moriarty, T. F.; Schwarz, E. M.; Muthukrishnan, G. Skeletal Infections: Microbial Pathogenesis, Immunity and Clinical Management. *Nat. Rev. Microbiol.* **2022**, *20* (7), 385−400.

(2) Kremers, H. M.; Nwojo, M. E.; Ransom, J. E.; Wood-Wentz, C. M.; Melton III, L. J.; Huddleston III, P. M. Trends in the

Epidemiology of Osteomyelitis: a Population-Based Study, 1969 to 2009. *J. Bone Joint Surg. Am.* **2015**, *97* (10), 837−845.
(3) Li, H.-K.; Rombach, I.; Zambellas, R.; Walker, A. S.; McNally, M. A.; Atkins, B. L.; Lipsky, B. A.; Hughes, H. C.; Bose, D.; Kümin, M.; et al. Oral Versus Intravenous Antibiotics for Bone and Joint Infection. *New Engl. J. Med.* **2019**, *380* (5), 425−436.
(4) Byrne, M. K.; Miellet, S.; McGlinn, A.; Fish, J.; Meedya, S.; Reynolds, N.; Van Oijen, A. M. The Drivers of Antibiotic Use and Misuse: the Development and Investigation of a Theory Driven Community Measure. *BMC Public Health* **2019**, *19*, 1−11.
(5) Ventola, C. L. The Antibiotic Resistance Crisis: Part 1: Causes and Threats. *Phar. Ther.* **2015**, *40* (4), 277.
(6) Ovington, L. Bacterial Toxins and Wound Healing. *Ostomy Wound Manag.* **2003**, *49* (7A Suppl), 8−12.
(7) Sun, Y.; Chan, J.; Bose, K.; Tam, C. Simultaneous Control of Infection and Inflammation with Keratin-Derived Antibacterial Peptides Targeting TLRs and Co-Receptors. *Sci. Transl. Med.* **2023**, *15* (686), No. eade2909.
(8) Park, H. Y.; Suh, G. Y.; Song, J.-U.; Yoo, H.; Jo, I. J.; Shin, T. G.; Lim, S. Y.; Woo, S.; Jeon, K. Early Initiation of Low-Dose Corticosteroid Therapy in the Management of Septic Shock: a Retrospective Observational Study. *Crit. Care* **2012**, *16*, 1−12.
(9) Ray, K. J.; Srinivasan, M.; Mascarenhas, J.; Rajaraman, R.; Ravindran, M.; Glidden, D. V.; Oldenburg, C. E.; Sun, C. Q.; Zegans, M. E.; McLeod, S. D.; et al. Early Addition of Topical Corticosteroids in the Treatment of Bacterial Keratitis. *JAMA Ophthalmol.* **2014**, *132* (6), 737−741.
(10) Aberdein, J.; Singer, M. Clinical Review: a Systematic Review of Corticosteroid Use in Infections. *Crit. Care* **2005**, *10*, 1−10.
(11) Feldman, C.; Anderson, R. Corticosteroids in the Adjunctive Therapy of Community-Acquired Pneumonia: an Appraisal of Recent Meta-Analyses of Clinical Trials. *J. Thorac. Dis.* **2016**, *8* (3), No. E162.
(12) Srinivasan, M.; Mascarenhas, J.; Rajaraman, R.; Ravindran, M.; Lalitha, P.; O'Brien, K. S.; Glidden, D. V.; Ray, K. J.; Oldenburg, C. E.; Zegans, M. E.; et al. The Steroids for Corneal Ulcers Trial (SCUT): Secondary 12-Month Clinical Outcomes of a Randomized Controlled Trial. *Am. J. Ophthalmol.* **2014**, *157* (2), 327−333.e3.
(13) Chu, H.; Pazgier, M.; Jung, G.; Nuccio, S.-P.; Castillo, P. A.; De Jong, M. F.; Winter, M. G.; Winter, S. E.; Wehkamp, J.; Shen, B.; et al. Human α-Defensin 6 Promotes Mucosal Innate Immunity through Self-Assembled Peptide Nanonets. *Science* **2012**, *337* (6093), 477−481.
(14) Weiss, G. L.; Stanisich, J. J.; Sauer, M. M.; Lin, C.-W.; Eras, J.; Zyla, D. S.; Trück, J.; Devuyst, O.; Aebi, M.; Pilhofer, M.; Glockshuber, R. Architecture and Function of Human Uromodulin Filaments in Urinary Tract Infections. *Science* **2020**, *369* (6506), 1005−1010.
(15) Fan, Y.; Li, X.-D.; He, P.-P.; Hu, X.-X.; Zhang, K.; Fan, J.-Q.; Yang, P.-P.; Zheng, H.-Y.; Tian, W.; Chen, Z.-M.; et al. A Biomimetic Peptide Recognizes and Traps Bacteria *in Vivo* As Human Defensin-6. *Sci. Adv.* **2020**, *6* (19), No. eaaz4767.
(16) Raetz, C. R. H.; Whitfield, C. Lipopolysaccharide Endotoxins. *Annu. Rev. Biochem.* **2002**, *71* (1), 635−700.
(17) Kimbrell, M. R.; Warshakoon, H.; Cromer, J. R.; Malladi, S.; Hood, J. D.; Balakrishna, R.; Scholdberg, T. A.; David, S. A. Comparison of the Immunostimulatory and Proinflammatory Activities of Candidate Gram-Positive Endotoxins, Lipoteichoic Acid, Peptidoglycan, and Lipopeptides, in Murine and Human Cells. *Immunol. Lett.* **2008**, *118* (2), 132−141.
(18) Kang, Y. J.; Kim, S. O.; Shimada, S.; Otsuka, M.; Seit-Nebi, A.; Kwon, B. S.; Watts, T. H.; Han, J. Cell Surface 4−1BBL Mediates Sequential Signaling Pathways' Downstream'of TLR and Is Required for Sustained TNF Production in Macrophages. *Nat. Immunol.* **2007**, *8* (6), 601−609.
(19) Durand, S. H.; Flacher, V.; Roméas, A.; Carrouel, F.; Colomb, E.; Vincent, C.; Magloire, H.; Couble, M.-L.; Bleicher, F.; Staquet, M.-J.; et al. Lipoteichoic Acid Increases TLR and Functional Chemokine Expression While Reducing Dentin Formation in *in Vitro* Differentiated Human Odontoblasts. *J. Immunol.* **2006**, *176* (5), 2880−2887.
(20) Martin, J. K.; Sheehan, J. P.; Bratton, B. P.; Moore, G. M.; Mateus, A.; Li, S. H.-J.; Kim, H.; Rabinowitz, J. D.; Typas, A.; Savitski, M. M.; et al. A Dual-Mechanism Antibiotic Kills Gram-Negative Bacteria and Avoids Drug Resistance. *Cell* **2020**, *181* (7), 1518−1532. e14.
(21) Wang, H.; Feng, Z.; Xu, B. Assemblies of Peptides in a Complex Environment and Their Applications. *Angew. Chem.* **2019**, *131* (31), 10532−10541.
(22) Levin, A.; Hakala, T. A.; Schnaider, L.; Bernardes, G. J.; Gazit, E.; Knowles, T. P. Biomimetic Peptide Self-Assembly for Functional Materials. *Nat. Rev. Chem.* **2020**, *4* (11), 615−634.
(23) Pappas, C. G.; Shafi, R.; Sasselli, I. R.; Siccardi, H.; Wang, T.; Narang, V.; Abzalimov, R.; Wijerathne, N.; Ulijn, R. V. Dynamic Peptide Libraries for the Discovery of Supramolecular Nanomaterials. *Nat. Nanotechnol.* **2016**, *11* (11), 960−967.
(24) Ding, Y.; Zheng, D.; Xie, L.; Zhang, X.; Zhang, Z.; Wang, L.; Hu, Z.-W.; Yang, Z. Enzyme-Instructed Peptide Assembly Favored by Preorganization for Cancer Cell Membrane Engineering. *J. Am. Chem. Soc.* **2023**, *145* (8), 4366−4371.
(25) Steiner, H.; Hultmark, D.; Engström, Å.; Bennich, H.; Boman, H. G. Sequence and Specificity of Two Antibacterial Proteins Involved in Insect Immunity. *Nature* **1981**, *292* (5820), 246−248.
(26) Helaine, S.; Kugelberg, E. Bacterial Persisters: Formation, Eradication, and Experimental Systems. *Trends Microbiol.* **2014**, *22* (7), 417−424.
(27) Flemming, H.-C.; Wingender, J.; Szewzyk, U.; Steinberg, P.; Rice, S. A.; Kjelleberg, S. Biofilms: an Emergent Form of Bacterial Life. *Nat. Rev. Microbiol.* **2016**, *14* (9), 563−575.
(28) Torres, M. D. T.; Melo, M. C.; Flowers, L.; Crescenzi, O.; Notomista, E.; de la Fuente-Nunez, C. Mining for Encrypted Peptide Antibiotics in the Human Proteome. *Nat. Biomed. Eng.* **2022**, *6* (1), 67−75.
(29) Song, M.; Liu, Y.; Huang, X.; Ding, S.; Wang, Y.; Shen, J.; Zhu, K. A Broad-Spectrum Antibiotic Adjuvant Reverses Multidrug-Resistant Gram-Negative Pathogens. *Nat. Microbiol.* **2020**, *5* (8), 1040−1050.
(30) Ding, X.; Yang, C.; Moreira, W.; Yuan, P.; Periaswamy, B.; de Sessions, P. F.; Zhao, H.; Tan, J.; Lee, A.; Ong, K. X.; et al. A Macromolecule Reversing Antibiotic Resistance Phenotype and Repurposing Drugs As Potent Antibiotics. *Adv. Sci.* **2020**, *7* (17), No. 2001374.
(31) Zhou, M.; Qian, Y.; Xie, J.; Zhang, W.; Jiang, W.; Xiao, X.; Chen, S.; Dai, C.; Cong, Z.; Ji, Z.; et al. Poly (2-Oxazoline)-Based Functional Peptide Mimics: Eradicating MRSA Infections and Persisters While Alleviating Antimicrobial Resistance. *Angew. Chem., Int. Ed.* **2020**, *59* (16), 6412−6419.
(32) Lei, J.; Wang, C.; Feng, X.; Ma, L.; Liu, X.; Luo, Y.; Tan, L.; Wu, S.; Yang, C. Sulfur-Regulated Defect Engineering for Enhanced Ultrasonic Piezocatalytic Therapy of Bacteria-Infected Bone Defects. *Chem. Eng. J.* **2022**, *435*, No. 134624.
(33) Shao, X.; Tian, Y.; Liu, J.; Yan, Z.; Ding, Y.; Hao, X.; Wang, D.; Shen, L.; Luo, E.; Guo, X. E.; et al. Rescuing SERCA2 Pump Deficiency Improves Bone Mechano-Responsiveness in Type 2 Diabetes by Shaping Osteocyte Calcium Dynamics. *Nat. Commun.* **2024**, *15* (1), No. 890.
(34) Li, J.; Ma, J.; Sun, H.; Yu, M.; Wang, H.; Meng, Q.; Li, Z.; Liu, D.; Bai, J.; Liu, G.; et al. Transformation of Arginine into Zero-Dimensional Nanomaterial Endows the Material with Antibacterial and Osteoinductive Activity. *Sci. Adv.* **2023**, *9* (21), No. eadf8645.
(35) Chen, D.; Zhou, Z.; Kong, N.; Xu, T.; Liang, J.; Xu, P.; Yao, B.; Zhang, Y.; Sun, Y.; Li, Y.; et al. Inhalable SPRAY Nanoparticles by Modular Peptide Assemblies Reverse Alveolar Inflammation in Lethal Gram-Negative Bacteria Infection. *Sci. Adv.* **2024**, *10* (37), No. eado1749.
(36) Han, M.-L.; Shen, H.-H.; Hansford, K. A.; Schneider, E. K.; Sivanesan, S.; Roberts, K. D.; Thompson, P. E.; Le Brun, A. P.; Zhu, Y.; Sani, M.-A.; et al. Investigating the Interaction of Octapeptin A3

https://doi.org/10.1021/acsnano.4c18858
ACS Nano XXXX, XXX, XXX−XXX

with Model Bacterial Membranes. *ACS Infect. Dis.* **2017**, *3* (8), 606−619.
(37) Cocker, D.; Birgand, G.; Zhu, N.; Rodriguez-Manzano, J.; Ahmad, R.; Jambo, K.; Levin, A. S.; Holmes, A. Healthcare As a Driver, Reservoir and Amplifier of Antimicrobial Resistance: Opportunities for Interventions. *Nat. Rev. Microbiol.* **2024**, *22*, 1−14.
(38) Qiao, Y.; Liu, X.; Li, B.; Han, Y.; Zheng, Y.; Yeung, K. W. K.; Li, C.; Cui, Z.; Liang, Y.; Li, Z.; et al. Treatment of MRSA-Infected Osteomyelitis Using Bacterial Capturing, Magnetically Targeted Composites with Microwave-Assisted Bacterial Killing. *Nat. Commun.* **2020**, *11* (1), No. 4446.
(39) Barry, A. L. An Overview of the Clinical and Laboratory Standards Institute (CLSI) and Its Impact on Antimicrobial Susceptibility Tests. In *Antimicrobial Susceptibility Testing Protocols* 2007; Vol. *1*.
(40) Standards, N. C. f. C. L.; Barry, A. L. *Methods for Determining Bactericidal Activity of Antimicrobial Agents: Approved Guideline*; National Committee for Clinical Laboratory Standards Wayne: PA, 1999; Vol. *19*.
(41) Lu, M.; Wang, S.; Wang, T.; Hu, S.; Bhayana, B.; Ishii, M.; Kong, Y.; Cai, Y.; Dai, T.; Cui, W.; Wu, M. X. Bacteria-Specific Phototoxic Reactions Triggered by Blue Light and Phytochemical Carvacrol. *Sci. Transl. Med.* **2021**, *13* (575), No. eaba3571.
(42) Nederberg, F.; Zhang, Y.; Tan, J. P.; Xu, K.; Wang, H.; Yang, C.; Gao, S.; Guo, X. D.; Fukushima, K.; Li, L.; et al. Biodegradable Nanostructures with Selective Lysis of Microbial Membranes. *Nat. Chem.* **2011**, *3* (5), 409−414.
(43) Cho, D.-I.; Kim, M. R.; Jeong, H.-y.; Jeong, H. C.; Jeong, M. H.; Yoon, S. H.; Kim, Y. S.; Ahn, Y. Mesenchymal Stem Cells Reciprocally Regulate the M1/M2 Balance in Mouse Bone Marrow-Derived Macrophages. *Exp. Mol. Med.* **2014**, *46* (1), e70.
(44) Stanley, E. R. Murine Bone Marrow-Derived Macrophages. *Basic Cell Culture Protocols* **1997**, *75*, 301−304.
(45) Assouvie, A.; Daley-Bauer, L. P.; Rousselet, G. Growing Murine Bone Marrow-Derived Macrophages. *Methods Molecular Biol.* **2018**, *1784*, 29−33.
(46) Das, P.; Sercu, T.; Wadhawan, K.; Padhi, I.; Gehrmann, S.; Cipcigan, F.; Chenthamarakshan, V.; Strobelt, H.; Dos Santos, C.; Chen, P.-Y.; et al. Accelerated Antimicrobial Discovery via Deep Generative Models and Molecular Dynamics Simulations. *Nat. Biomed. Eng.* **2021**, *5* (6), 613−623.
(47) Kalienkova, V.; Peter, M. F.; Rheinberger, J.; Paulino, C. Structures of a Sperm-Specific Solute Carrier Gated by Voltage and cAMP. *Nature* **2023**, *623* (7985), 202−209.
(48) Makhlouf, L.; Peter, J. J.; Magnussen, H. M.; Thakur, R.; Millrine, D.; Minshull, T. C.; Harrison, G.; Varghese, J.; Lamoliatte, F.; Foglizzo, M.; et al. The UFM1 E3 Ligase Recognizes and Releases 60S Ribosomes from ER Translocons. *Nature* **2024**, *627* (8003), 437−444.
(49) Kim, W.; Zhu, W.; Hendricks, G. L.; Van Tyne, D.; Steele, A. D.; Keohane, C. E.; Fricke, N.; Conery, A. L.; Shen, S.; Pan, W.; et al. A New Class of Synthetic Retinoid Antibiotics Effective against Bacterial Persisters. *Nature* **2018**, *556* (7699), 103−107.

https://doi.org/10.1021/acsnano.4c18858
ACS Nano XXXX, XXX, XXX−XXX